ELSEVIER

Marine Geology 236 (2007) 121 – 141

MARINE GEOLOGY
INTERNATIONAL JOURNAL OF MARINE GEOLOGY, GEOCHEMISTRY AND GEOPHYSICS

www.elsevier.com/locate/margeo

# Origin of basal dolomitic claystone in the Marsili Basin, Tyrrhenian Sea

Vesselin M. Dekov [a], George D. Kamenov [b,*], Carlo Savelli [c], Jens Stummeyer [d], Vesna Marchig [d]

[a] *Department of Geology and Paleontology, University of Sofia, 15 Tzar Osvoboditel Blvd., 1000 Sofia, Bulgaria*
[b] *Department of Geological Sciences, University of Florida, 241 Willamson Hall, Gainesville, FL 32611, USA*
[c] *Istituto di Geologia Marina, CNR, Via Gobetti 101, 40129 Bologna, Italy*
[d] *Bundesanstalt für Geowissenschaften und Rohstoffe, Stilleweg 2, D-30655 Hannover, Germany*

Received 6 April 2006; received in revised form 28 August 2006; accepted 1 October 2006

**Abstract**

Red–brown dolomitic claystones overlay the Marsili Basin basaltic basement at ODP Site 650. Sequential leaching experiments reveal that most of the elements considered to have a hydrothermal or hydrogenous origin in a marine environment, such as Fe, Cu, Zn, Pb, Co, Ni, are present mainly in the aluminosilicate fraction of the dolomitic claystones. Their vertical distribution, content and partitioning chemistry of trace elements, and REE patterns suggest enhanced terrigenous input during dolomite formation, but no significant hydrothermal influence from the underlying basaltic basement.

Positive correlations in the C and O isotopes in the dolomites reflect complex conditions during the dolomitization. The stable isotopes can be controlled in part by temperature variations during the dolomitization. Majority of the samples, however, form a trend that is steeper than expected for only temperature control on the C and O isotopes. The latter indicates possible isotopic heterogeneity in the proto-carbonate that can be related to arid climatic conditions during the formation of the basal dolomitic claystones. In addition, the dolostones stable isotopic characteristics can be influenced by diagenetic release of heavier $\delta^{18}O$ from clay dehydration and/or alteration of siliciclastic material. Strontium and Pb isotopic data reveal that the non-carbonate fraction, the "dye" of the dolomitic claystones, is controlled by Saharan dust (75%–80%) and by material with isotopic characteristics similar to the Aeolian Arc volcanoes (20%–25%). The non-carbonate fraction of the calcareous ooze overlying the dolomitic claystones has a Sr and Pb isotopic composition identical to that of the dolomitic claystones, indicating that no change in the input sources to the sedimentary basin occurred during and after the dolomitization event.

Combination of climato-tectonic factors most probably resulted in suitable conditions for dolomitization in the Marsili and the nearby Vavilov Basins. The basal dolomitic claystone sequence was formed at the initiation of the opening of the Marsili Basin (~2 Ma), which coincided with the consecutive glacial stage. The glaciation caused arid climate and enhanced evaporation that possibly contributed to the stable isotope variations in the proto-carbonate. The conductive cooling of the young lithosphere produced high heat flow in the region, causing low-temperature passive convection of pore waters in the basal calcareous sediment. We suggest that this pumping process was the major dolomitization mechanism since it is capable of driving large volumes of seawater (the source of $Mg^{2+}$) through the sediment. The red–brown hue of the dolomitic claystones is terrigenous contribution of the glacially induced high eolian influx and was not hydrothermally derived from the underlying basaltic basement. The detailed geochemical investigation of the basal dolomitic sequence indicates that the

* Corresponding author. Tel.: +1 352 846 3955; fax: +1 352 392 9294.
*E-mail address:* kamenov@ufl.edu (G.D. Kamenov).

0025-3227/$ - see front matter 
doi:10.1016/j.margeo.2006.10.021

dolomitization was most probably related to complex tectono-climatic conditions set by the initial opening stages of the Marsili Basin and glaciation.


*Keywords:* dolomitic claystones; metalliferous sediments; glaciation; Marsili Basin; Tyrrhenian Sea

## 1. Introduction

ODP Site 650 A (Leg 107; the Marsili Basin) drilled brightly coloured basal sediments, composed of Ca-dolomites enriched in Fe and Mn, similar to the dolomites overlying the igneous basement in the nearby Vavilov Basin (McKenzie et al., 1990; Robertson, 1990). McKenzie et al. (1990) suggested that Mg-enriched solutions, that dolomitized the Tyrrhenian basal carbonates, could have been derived from the reaction of circulating seawater with the underlying basic rocks. These Mg-rich hydrothermal solutions should be a product of low-temperature reactions (McKenzie et al., 1990) because seawater-rock interactions between 70 and 500 °C lead to total removal of Mg into the alteration by-products (Mottl, 1983). Although plausible, the above model of dolomitization invokes some questions, including were the tepid solutions capable of leaching enough Mg as well as Fe and Mn from the underlying crust and if the "ferruginous dolostone" sequence is a product of metasomatism, is there upward gradual decrease in the content of elements considered to be hydrothermal? In addition, in order to decipher the origin of these "ferruginous dolostones" important questions that need to be investigated include the source of Mg, Fe, and Mn, their transport through/to the basal carbonate sequence, and conditions of dolomitization. Another possibility that also needs to be addressed is if there is a link between the formation of the basal "ferruginous dolostones" and the climatic and tectonic changes during the glacial events at the Late Pliocene/Early Pleistocene and the opening of the Marsili Basin. In order to shed more light on these questions, we conducted detailed geochemical study of the basal "ferruginous dolostone"

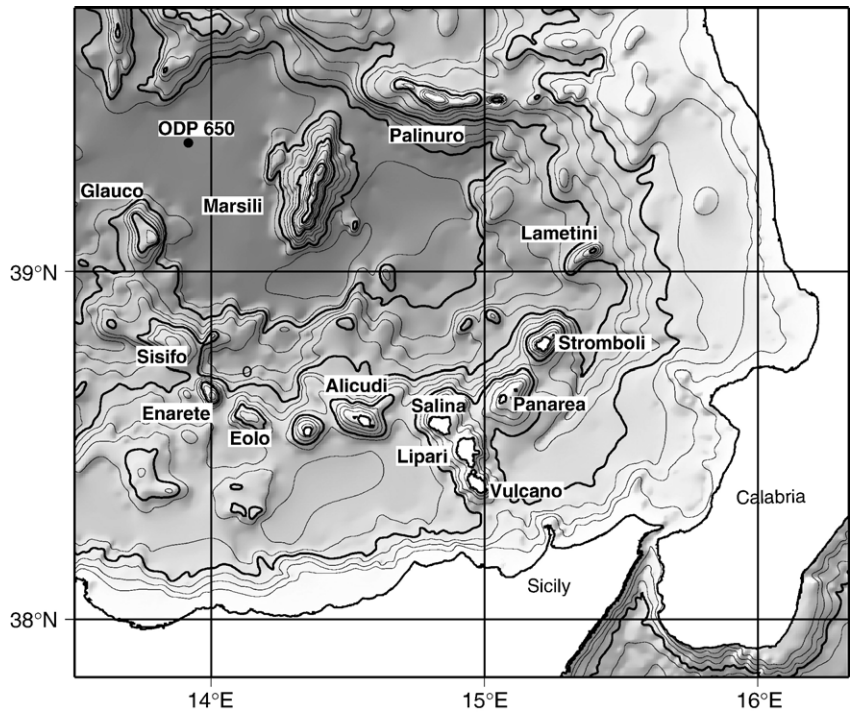


Fig. 1. Location of ODP Site 650 that penetrated the oceanic crust to the west of Marsili Seamount. Bold bathymetric lines indicate depths of 1000, 2000 and 3000 m. The volcanic islands and seamounts of the Aeolian Arc are bordered by the orocline of crystalline-metamorphic rocks which extends from NE Sicily (Peloritani Mounts) to Calabria (up to about the latitude of Palinuro volcano, 39°30′ N).

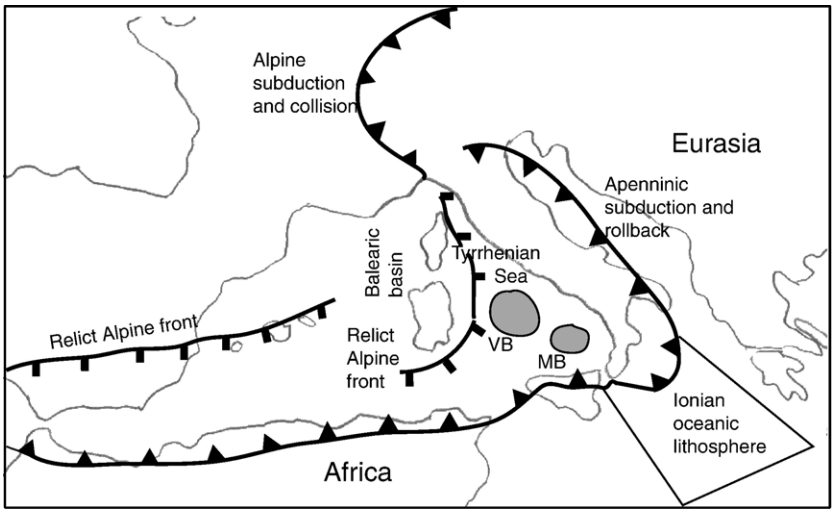


Fig. 2. Schematic outline of the relict and active Alpine fronts of subduction-collision and of the boundary of Apenninic rollback in the west Mediterranean. Light shading shows the small back-arc basins of Vavilov (VB) and Marsili (MB) of south Tyrrhenian Sea, which are floored by oceanic lithosphere generated by retreat of old subducted Ionian lithosphere.

unit in the Marsili Basin and its possible relation to the climatic changes and early spreading pulse in the basin.

## 2. Geological setting

The Tyrrhenian Sea was formed as a result of back-arc spreading above a northwest dipping subduction zone during the Pliocene. Marsili Basin includes the eastern portion of the south Tyrrhenian oceanic lithosphere and is located between the Aeolian calcalkaline volcanic region and the older Vavilov Basin (~8 Ma) to the west (Figs 1 and 2). A large, approximately N–S aligned volcanic seamount occupies the basin central part. Rapid magmatic emplacement of basaltic lavas with tholeiitic to calcalkaline transitional affinity formed the Marsili oceanic lithosphere about 1.9–1.6 Ma (Argnani and

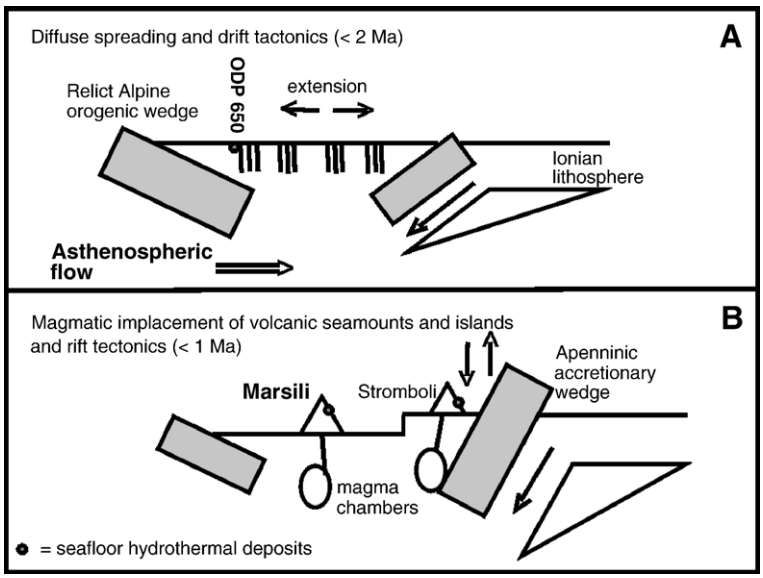


Fig. 3. Cartoon showing relationships between hydrothermal processes, volcanism and tectonics in SE Tyrrhenian: (A) extension and magmatic emplacement of dikes (diffuse spreading); (B) hydrothermal deposits of Fe–Mn-oxyhydroxides and polymetallic sulfides are associated with rifting and volcanism at the seamounts overlying magma chambers.

Savelli, 1999). This portion of new oceanic lithosphere was emplaced within the stretched and thinned south Tyrrhenian Alpine/Apenninic orogenic domain. Although the Marsili spreading event was short-lived and localized, it had regional Tyrrhenian–Perityrrhenian geological significance because it is difficult to find coeval magmatic manifestations outside the small, deep basin. Later on, around 0.8 Ma ago, voluminous volcanic activity formed several large volcanic seamounts and islands in the SE Tyrrhenian Sea region. The period of seamount formation (~0.8–0 Ma) was characterized by both rifting tectonics and magmatic emplacement of calcalkaline lavas. Intense vertical tectonics and magmatism probably caused rapid subsidence (~1 km/Ma) of the newly formed oceanic lithosphere and its adjacent continental margins. This geodynamic framework, with its high geothermal gradient and deep-seated normal faulting, was favourable for enhanced hydrothermal circulation (Fig. 3; Dekov and Savelli, 2004).

## 3. Material and methods

Approximately 2.1 m of a basal "ferruginous dolostone" unit were recovered by drilling in contact with the underlying basalt (Fig. 4). A 10-cm pale greenish grey dolomitic layer separates the vesicular basalt from the overlaying pale brown to reddish brown "ferruginous dolostone". Nine samples from the basal dolomitic sequence were selected for this study, including a sample from the greenish grey "dolostone" from the sediment/basalt contact, 7 of the overlaying reddish brown "ferruginous dolostone" and 1 background reference sample of the overlying undolomitized greenish grey nannofossil ooze (Fig. 4; Table 1). Samples were selected on the basis of lithology and colour. Prior to the analyses, the samples were ground and washed with distilled water to remove interstitial soluble salts. Then, the sediments were centrifuged in order to settle down the fine Fe-oxyhydroxide suspension and were dried in an oven at 30 °C.

Carbon was determined on duplicate bulk samples using a FISON NA2000 Element Analyzer after removal of the carbonate fraction by dissolution with 1.5 N HCl in an Ag capsule (Table 1). Bulk X-ray diffraction (XRD) analyses were made on powdered specimens, using a Philips PW1730 diffractometer (Cu $K_\alpha$ radiation, Ni filter, 40 kV, 20 mA, scans from 2 to 70°2$\theta$, scan velocity of 1°2$\theta$/min). Detrital quartz, present in all samples, was used as an internal standard. The separated clay fraction (<2 μm) was investigated by XRD on 3 types of oriented mounts: air-dried, glycol-saturated and after heating of air-dried mounts to 550 °C, from 2 to 40°2$\theta$, steps of 0.02°2$\theta$,

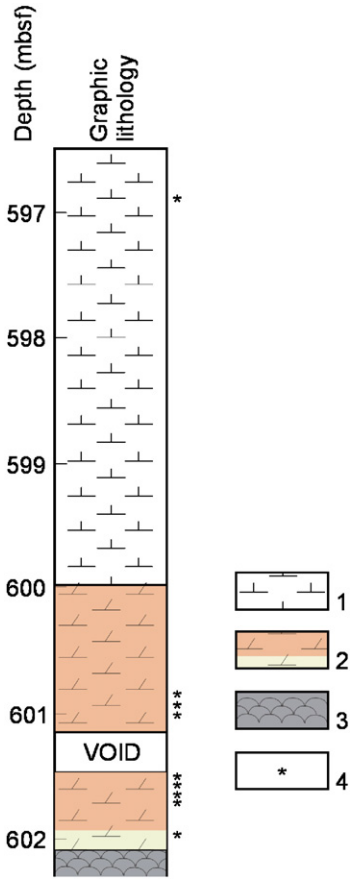


Fig. 4. Schematic sedimentary log of the studied lower part of ODP Site 650A. 1 = nannofossil ooze; 2 = dolomitic claystone; 3 = basaltic basement; 4 = sample positions.

at 1 s/step. Randomly oriented specimens were produced (57–64°2$\theta$ scans, steps of 0.02°2$\theta$, at 120 s/step) to identify di- or trioctahedral clay minerals from 060 reflections. The carbonate percentage in the bulk samples (Table 1) was estimated assuming that all $C_{inorg}$ (Table 1) is carbonate crystal lattice bound. The mole fraction of $MgCO_3$ in the dolomite was estimated measuring the shift of the major dolomite peak {10.4} relative to that of the quartz {10.1}. The measured difference in d-spacing was used to obtain the mol% Mg in the dolomite crystal lattice (Table 1) (Lumsden, 1979). The degree of order in the dolomite crystal lattice was estimated from the $I_{015}/I_{110}$ ratio (Füchtbauer and Goldschmidt, 1965) and the shape of the superstructural peaks {021}, {015} and {101} (Graf and Goldsmith, 1956). Scanning electron microscope (SEM) observations were made on Au-coated fragments of bulk natural samples using a JEOL JSM-5410LV electron microscope. Infra red (IR) spectra were recorded on KBr/sample pellets (200 mg/1 mg) with Specord 75 IR unit.

Table 1
Mineralogical composition (XRD) and C content of the studied samples

| Sample identification: | Work # | Depth | $C_{tot}$ | $C_{org}$ | $C_{inorg}$ | Bulk mineralogy[a] | | | | | | | Clay mineralogy (<2 μ) (%)[b] | | | | | | |
|---|---|---|---|---|---|---|---|---|---|---|---|---|---|---|---|---|---|---|---|
| Leg–Hole–Core–Section (Horizon) | | (mbsf) | (%) | (%) | (%) | Dolomite (%) | Mg in dolomite (mol%) | $I_{015}/I_{110}$ | Calcite (%) | Quartz | Plagioclase | Mica | Analcite | Smectite | Illite | Kaolinite | Chlorite | $n_\alpha$ | V/$p$ |
| 107–650A–65X–1 (50–53) | 9 | 596.89 | 5.94 | 0.12 | 5.82 | | 1.0 | – | **** 48.50 | *** | * | ** | | 14 | 52 | 18 | 16 | 7.0 | 0.38 |
| 107–650A–66X–1 (98–100) | 8 | 600.86 | 5.28 | 0.07 | 5.21 | **** 40.0 | 44.0 | 0.79 | | *** | ** | ** | | 35 | 52 | 8 | 5 | 6.0 | 0.56 |
| 107–650A–66X–1 (104–106) | 7 | 600.92 | 5.31 | 0.06 | 5.25 | **** 40.3 | 44.0 | 0.95 | | *** | ** | ** | | 39 | 48 | 9 | 4 | 7.0 | 0.54 |
| 107–650A–66X–1 (112–114) | 6 | 601.00 | 5.20 | 0.06 | 5.14 | **** 39.5 | 43.3 | 0.91 | | *** | ** | ** | | 35 | 49 | 10 | 6 | 5.5 | 0.54 |
| 107–650A–66X–2 (2–4) | 5 | 601.40 | 5.48 | 0.07 | 5.41 | **** 41.5 | 43.3 | 0.63 | | *** | ** | ** | | 41 | 49 | 10 | traces | 6.5 | 0.60 |
| 107–650A–66X–2 (7–9) | 4 | 601.45 | 5.99 | 0.04 | 5.95 | **** 45.7 | 44.0 | 0.94 | | *** | ** | ** | | 42 | 49 | 9 | –"– | 8.5 | 0.60 |
| 107–650A–66X–2 (14–16) | 3 | 601.52 | 4.06 | 0.05 | 4.01 | **** 30.8 | 44.0 | 0.95 | | *** | ** | ** | | 43 | 49 | 8 | –"– | 7.5 | 0.55 |
| 107–650A–66X–2 (21–23) | 2 | 601.59 | 3.73 | 0.05 | 3.68 | **** 28.3 | 44.0 | 0.93 | | *** | ** | ** | | 48 | 41 | 11 | –"– | 7.5 | 0.52 |
| 107–650A–66X–2 (56–59) | 1 | 601.94 | 4.42 | 0.05 | 4.37 | **** 33.5 | 44.0 | 0.81 | | *** | ** | ** | * | 73 | 22 | 5 | –"– | 8.5 | 0.82 |

[a] Abundance codes: **** — abundant; *** — frequent; **— rare; * — present.
[b] The individual clay mineral percentages are expressed in terms of a 100% clay mineral sample; i.e., (smectite+illite+kaolinite+chlorite)=100%.

The determination of the total element concentrations of the samples was performed with X-ray fluorescence spectrometry (XRF) and Inductively Coupled Plasma Mass Spectrometry (ICP-MS). XRF analyses were performed using Philips PW 2400 and PW 1480 wavelength dispersive spectrometers. 42 major and trace elements were quantitatively analysed after fusion of 1g sample material with lithiummetaborate at 1200 °C for 20 min (sample/$Li_2B_4O_7$=1/5). Quality of the results was controlled with certified reference materials (CRM) (i.e., BCR, Community Bureau of Reference, Brussels). This procedure ensures an analytical precision better than +/−0.5% relative for major elements and 1–10 ppm for trace elements (analytical precision for XRF analyses of certified reference materials). Trace element and rare earth element (REE) concentrations of the samples were analysed with ICP-MS (Perkin Elmer Sciex Elan 5000) after wet chemical decomposition of the samples in a closed microwave system: 0,5 g of the sample was heated with 3 ml HF and 1 ml $HNO_3$ (both suprapure quality). After decomposition the clear solutions were treated with 70% $HClO_4$ to remove HF. Completeness of the decomposition procedure for REE was controlled by analyzing CRM (e.g. USGS rock standards AGV-1 and G-2). For REE determination the relative standard deviation (RSD) based on triplicate analyses of CRM was found to be in the range of 1% for light REE (>10 ppm) and up to 10% for heavy REE at trace levels (<1 ppm). To minimize isobaric interferences the instrument conditions were set to produce a minimal signal of $BaO^+$ while analysing a standard solution of 10 ppm Ba. While the rate of oxide formation was below 0.5% no further interference correction was applied. Instrument calibration was performed with multi-element solutions similar to sample composition. Long term stability of the instrument was controlled periodically using NIST CRM 1643d. Under these conditions a RSD of approximately 5% was achieved for multi-element determination at trace levels.

The phase distribution of elements was determined in a three-step sequential extraction procedure (Davidson et al., 1994): (1) Exchangeable adsorbed elements, carbonates, and carbonate bound elements: 0.5 g of powdered dried sample was treated with 20 ml of 0.1 M acetic acid solution in a PTFA centrifuge tube for 5 h at room temperature. After centrifugation the liquid phase was separated and the residue was washed with water. (2) Easily reducible fraction (including Mn-oxides and co-precipitated elements): the residue of step 1 was treated with 20 ml of 0.1 M hydroxylamine–hydrochloride solution ($NH_2OH$/HCl; pH=2). The sample was shaken for 6 h at room temperature. The residue was again centrifuged and washed with water. (3) Oxidizeable phases, organic matter and sulphides: the residue of step 2 was treated twice with 10 ml 8.8 M hydrogen peroxide ($H_2O_2$) at a temperature of 85 °C. All reagents used were of suprapure or pro analytical grade. Possible contamination of the resulting solutions was checked using reagent blanks. The solutions of the leaching steps were diluted with water to a volume of 50 ml. Element concentrations were analysed using ICP-OES (Jobin Yvon JY 166 Ultrace). The standard deviation of ICP-OES measurements was generally better than 10%, determined by multiple extractions of selected samples.

Finnegan MAT 252 mass spectrometer equipped with an online automated carbonate preparation system was used for the O and C isotope analyses. Dolomite data were corrected for fractionation (a result of $H_3PO_4$ dissolution at 90 °C) using an alpha value of 1.00932 (Rosenbaum and Sheppard, 1986). For Sr and Pb isotope analyses about 0.1 g powders were dissolved in a mixture of HF+$HNO_3$. Sr was separated using standard chromatographic methods on Dowex 50 X12 cation exchange resin. The Sr isotope analyses were performed on a Micromass Sector 54 Thermal Ionization mass spectrometer equipped with seven Faraday and one Daly collectors. Sr samples were loaded on oxidized tungsten single filaments and run in dynamic mode. Data were acquired at a beam intensity of around 1.5 V $^{88}Sr$, with corrections for instrumental discrimination made assuming $^{86}Sr/^{88}Sr=0.1194$. Errors in measured $^{87}Sr/^{86}Sr$ are better than +/−0.00002 (2σ) based on long-term reproducibility of NBS 987 ($^{87}Sr/^{86}Sr=0.71024$). Lead was separated and purified in HBr medium following standard chromatographic techniques. Pb isotope analyses were conducted on Nu-Plasma multi collector ICP-MS (Nu Instruments, UK) using Tl for mass-bias correction, for more details see Kamenov et al. (2004) and Kamenov et al. (2005). The reported Pb isotopic compositions are relative to the following NBS 981 values: $^{206}Pb/^{204}Pb=16.9369$ (+/−0.0039, 2 se), $^{207}Pb/^{204}Pb=15.4904$ (+/−0.0034, 2 se), and $^{208}Pb/^{204}Pb=36.6949$ (+/−0.0087, 2 se).

## 4. Results

### 4.1. Mineralogy

The carbonate component in all 8 “dolostone” samples was 100% dolomite whereas in the background sample it was 100% calcite (Table 1). Low-Mg calcite makes up around 50% of the background nannofossil oozes (Table 1).

Table 2
Chemical composition of investigated sediments

| Work # | Depth (mbsf) | Si wt.% | Ti | Al | Fe | $Fe_{CFB}$ | Mn | $Mn_{CFB}$ | Mg | Ca | Na | K | P | LOI | Al/(Al+Fe+Mn) | As ppm | Ba | Be | Bi | Cd | Co |
|---|---|---|---|---|---|---|---|---|---|---|---|---|---|---|---|---|---|---|---|---|---|
| 9 | 596.89 | 13.1 | 0.27 | 2.65 | 1.07 | 2.08 | 0.21 | 0.41 | 1.07 | 19.2 | 0.18 | 0.70 | 0.02 | 26.9 | 0.67 | 6.0 | 136 | 0.94 | 0.06 | 0.01 | 13.1 |
| 8 | 600.86 | 15.1 | 0.28 | 2.68 | 2.05 | 3.42 | 0.76 | 1.27 | 4.96 | 9.99 | 0.16 | 0.81 | 0.02 | 25.3 | 0.49 | 8.6 | 138 | 1.17 | 0.05 | 0.10 | 19.5 |
| 7 | 600.92 | 15.2 | 0.28 | 2.68 | 2.08 | 3.48 | 0.74 | 1.24 | 4.91 | 9.90 | 0.27 | 0.81 | 0.02 | 25.1 | 0.49 | 8.7 | 144 | 1.03 | 0.07 | 0.08 | 19.2 |
| 6 | 601.00 | 15.0 | 0.27 | 2.66 | 2.08 | 3.44 | 0.75 | 1.24 | 4.96 | 9.95 | 0.23 | 0.80 | 0.02 | 25.4 | 0.48 | 8.3 | 134 | 1.04 | 0.04 | 0.11 | 19.5 |
| 5 | 601.40 | 14.2 | 0.26 | 2.53 | 2.19 | 3.75 | 0.70 | 1.20 | 5.15 | 10.5 | 0.25 | 0.75 | 0.02 | 26.3 | 0.47 | 9.1 | 143 | 1.16 | 0.06 | 0.12 | 21.7 |
| 4 | 601.45 | 13.9 | 0.26 | 2.48 | 2.10 | 3.87 | 0.72 | 1.33 | 5.28 | 10.9 | 0.15 | 0.77 | 0.02 | 26.8 | 0.47 | 8.1 | 125 | 1.19 | 0.04 | 0.12 | 22.7 |
| 3 | 601.52 | 16.4 | 0.30 | 2.98 | 2.73 | 3.94 | 0.53 | 0.77 | 4.30 | 7.95 | 0.31 | 0.90 | 0.03 | 22.9 | 0.48 | 10.9 | 132 | 1.19 | 0.11 | 0.08 | 18.5 |
| 2 | 601.59 | 16.9 | 0.31 | 3.08 | 2.79 | 3.89 | 0.50 | 0.70 | 4.17 | 7.45 | 0.29 | 0.93 | 0.03 | 22.3 | 0.48 | 11.2 | 128 | 1.36 | 0.09 | 0.08 | 17.8 |
| 1 | 601.94 | 14.5 | 0.27 | 2.70 | 1.67 | 2.51 | 0.84 | 1.26 | 5.11 | 10.2 | 0.27 | 0.62 | 0.01 | 26.3 | 0.52 | 74.9 | 95 | 1.12 | 0.01 | 0.90 | 162.0 |

| Work # | Depth (mbsf) | Cr ppm | Cs | Cu | Ga | Ge | Hf | Li | Mo | Nb | Ni | Pb | Rb | Sb | Sc | Sn | Sr | Ta | Th | Tl | U | V | W | Zn | Zr |
|---|---|---|---|---|---|---|---|---|---|---|---|---|---|---|---|---|---|---|---|---|---|---|---|---|---|
| 9 | 596.89 | 63 | 4.3 | 43.2 | 11.2 | 0.71 | 1.7 | 26.2 | 0.32 | 9.5 | 25.5 | 28.0 | 77.6 | 1.01 | 8.7 | 1.7 | 857 | 0.79 | 6.1 | 0.44 | 2.2 | 98 | 1.3 | 61 | 86 |
| 8 | 600.86 | 63 | 4.4 | 20.3 | 12.0 | 0.98 | 1.9 | 17.2 | 1.17 | 9.9 | 54.6 | 26.7 | 83.3 | 0.78 | 9.0 | 1.7 | 127 | 0.88 | 6.3 | 0.34 | 1.2 | 87 | 1.4 | 75 | 86 |
| 7 | 600.92 | 63 | 4.3 | 22.6 | 12.0 | 1.03 | 1.8 | 17.1 | 1.20 | 9.8 | 55.4 | 26.9 | 83.6 | 0.77 | 9.0 | 1.8 | 129 | 0.88 | 6.2 | 0.35 | 1.1 | 89 | 1.7 | 72 | 90 |
| 6 | 601.00 | 60 | 4.3 | 19.5 | 12.1 | 1.03 | 1.8 | 17.0 | 1.18 | 9.5 | 54.4 | 28.0 | 82.1 | 0.82 | 9.1 | 1.7 | 130 | 0.91 | 6.1 | 0.33 | 1.1 | 87 | 1.3 | 75 | 89 |
| 5 | 601.40 | 57 | 4.2 | 21.0 | 12.2 | 0.97 | 1.7 | 15.7 | 1.43 | 9.2 | 53.9 | 19.4 | 81.2 | 0.90 | 8.9 | 1.6 | 132 | 0.96 | 5.8 | 0.33 | 1.1 | 80 | 1.8 | 74 | 87 |
| 4 | 601.45 | 53 | 4.2 | 17.8 | 11.7 | 0.93 | 1.7 | 15.0 | 1.27 | 9.2 | 51.6 | 18.5 | 79.9 | 0.84 | 8.8 | 1.6 | 133 | 1.10 | 5.9 | 0.34 | 1.1 | 76 | 1.4 | 68 | 86 |
| 3 | 601.52 | 65 | 4.5 | 24.6 | 14.0 | 1.20 | 2.0 | 20.0 | 1.90 | 9.5 | 64.3 | 18.4 | 88.9 | 1.21 | 10.3 | 1.8 | 121 | 1.13 | 6.3 | 0.36 | 1.1 | 89 | 2.0 | 77 | 89 |
| 2 | 601.59 | 70 | 4.6 | 24.8 | 14.7 | 1.24 | 2.0 | 22.4 | 2.00 | 9.8 | 69.7 | 20.3 | 90.2 | 1.33 | 11.4 | 1.9 | 120 | 1.19 | 6.3 | 0.38 | 1.1 | 91 | 2.0 | 78 | 91 |
| 1 | 601.94 | 71 | 3.0 | 602.0 | 11.4 | 0.90 | 1.8 | 18.7 | 0.97 | 7.4 | 238.0 | 40.2 | 60.2 | 1.66 | 15.4 | 1.4 | 143 | 1.23 | 5.1 | 0.85 | 5.7 | 132 | 1.0 | 139 | 81 |

| Work # | Depth (mbsf) | Y ppm | La | Ce | Pr | Nd | Sm | Eu | Gd | Tb | Dy | Ho | Er | Tm | Yb | Lu | ΣREE | $(Ce/Ce^*)^a$ | $(Eu/Eu^*)^b$ | $La_N/Lu_N$ | $(Nd/Fe)^c$ |
|---|---|---|---|---|---|---|---|---|---|---|---|---|---|---|---|---|---|---|---|---|---|
| 9 | 596.89 | 13.1 | 20.4 | 40.8 | 4.74 | 17.8 | 3.40 | 0.70 | 3.21 | 0.46 | 2.43 | 0.49 | 1.43 | 0.20 | 1.32 | 0.21 | 97.6 | 0.95 | 0.99 | 1.04 | 166.3 E−05 |
| 8 | 600.86 | 14.6 | 21.4 | 42.8 | 4.95 | 18.5 | 3.60 | 0.77 | 3.39 | 0.49 | 2.68 | 0.52 | 1.52 | 0.22 | 1.35 | 0.22 | 102.4 | 0.95 | 1.03 | 1.04 | 90.2 E−05 |
| 7 | 600.92 | 14.5 | 21.2 | 42.2 | 4.91 | 18.5 | 3.47 | 0.75 | 3.35 | 0.46 | 2.65 | 0.51 | 1.51 | 0.21 | 1.36 | 0.21 | 101.3 | 0.94 | 1.03 | 1.08 | 88.9 E−05 |
| 6 | 601.00 | 14.5 | 20.9 | 41.5 | 4.81 | 18.1 | 3.43 | 0.76 | 3.21 | 0.47 | 2.57 | 0.51 | 1.53 | 0.21 | 1.31 | 0.21 | 99.5 | 0.94 | 1.07 | 1.06 | 87.0 E−05 |
| 5 | 601.40 | 12.9 | 19.8 | 39.7 | 4.54 | 17.2 | 3.23 | 0.70 | 3.03 | 0.44 | 2.38 | 0.49 | 1.41 | 0.20 | 1.24 | 0.20 | 94.6 | 0.95 | 1.05 | 1.06 | 78.5 E−05 |
| 4 | 601.45 | 13.0 | 19.7 | 40.0 | 4.60 | 17.4 | 3.24 | 0.70 | 2.99 | 0.44 | 2.46 | 0.47 | 1.43 | 0.20 | 1.28 | 0.20 | 95.1 | 0.96 | 1.06 | 1.05 | 82.9 E−05 |
| 3 | 601.52 | 12.8 | 19.7 | 38.9 | 4.58 | 17.0 | 3.13 | 0.70 | 2.90 | 0.42 | 2.38 | 0.46 | 1.39 | 0.20 | 1.28 | 0.21 | 93.3 | 0.93 | 1.09 | 1.00 | 62.3 E−05 |
| 2 | 601.59 | 13.2 | 20.3 | 39.5 | 4.69 | 17.5 | 3.30 | 0.71 | 2.97 | 0.44 | 2.47 | 0.51 | 1.45 | 0.21 | 1.33 | 0.22 | 95.6 | 0.92 | 1.07 | 0.98 | 62.7 E−05 |
| 1 | 601.94 | 23.0 | 19.9 | 40.8 | 4.86 | 19.1 | 3.98 | 1.02 | 4.02 | 0.63 | 3.97 | 0.82 | 2.52 | 0.38 | 2.54 | 0.42 | 105.0 | 0.95 | 1.19 | 0.51 | 114.4 E−05 |

[a] $Ce/Ce^* = 2Ce_N/(La_N + Pr_N)$.
[b] $Eu/Eu^* = 2Eu_N/(Sm_N + Gd_N)$.
[c] Read 88.9 E−05 as $88.9 \times 10^{-5}$.

The dolomite is dominated by small (1–10 μm), euhedral Ca-dolomite crystals (SEM observations). No mixed Ca–Mg–Fe–Mn carbonates (XRD- and IR-distinguishable) could be identified. Quartz, plagioclase, and mica are subordinate components, but present throughout the studied sequence. Dolomite content is highest in the middle/upper "dolostone" section. The mole fraction of $MgCO_3$ in the dolomite samples shows no significant variation (Table 1). Although variable, the degree of order of the dolomite crystal lattice is high, $I_{015}/I_{110}$=0.63–0.95 with well-shaped sharp superstructural peaks {021}, {015}, {101}. Lowermost, uppermost, and the middle samples of the "dolostone" sequence exhibit the least degree of ordering (Table 1).

Clays are the other main constituent of the "dolostones" (Table 1), suggesting that the latter could be more precisely named "dolomitic claystones". Clay minerals are mainly smectite and illite with minor amounts of chlorite and kaolinite (XRD patterns available on request). Smectite is the dioctahedral Fe–Mg variety: montmorillonite. The proportions and content of the clay minerals in the nannofossil oozes reflects the background terrigenous input. Illite makes up about half of the clay fraction and each of the other 3 clay minerals have comparable proportions (Table 1). Illite content decreases down through the reddish brown dolomitic claystones whereas smectite increases downhole and reaches maximum content in the lowermost greenish

Table 3
Phase distribution of elements

| Work # | Depth (mbsf) | Phase[a] | Al ppm | Ba | Ca | Cd | Co | Cr | Cu | Fe | Mg | Mn | Ni | Pb | Sr | Zn |
|---|---|---|---|---|---|---|---|---|---|---|---|---|---|---|---|---|
| 9 | 596.89 | 1 | 10.7 | 3.26 | 88155 | 0.18 | 1.0 | 0.03 | 2.77 | 0 | 964 | 604 | 0.84 | <0.5 | 541 | 1.28 |
| | | 2 | 40.7 | 3.73 | | <0.10 | 0.1 | 0.06 | 5.40 | 138 | 207 | 348 | 0.04 | 0.67 | 262 | 1.48 |
| | | 3 | 143 | 2.18 | 39618 | 2.18 | 2.1 | 0.96 | 16.4 | 1190 | 1998 | 878 | 1.33 | 11.7 | 132 | 5.46 |
| | | 4 | 26305 | 127 | | 0 | 9.9 | 61.9 | 18.6 | 9374 | 7563 | 253 | 23.3 | 15.7 | 0 | 52.8 |
| 8 | 600.86 | 1 | 28.5 | 3.26 | 43959 | 0.16 | 6.4 | 0.31 | 1.82 | 1502 | 18048 | 4164 | 6.88 | <0.5 | 61.7 | 9.43 |
| | | 2 | 52.8 | 3.29 | 29628 | <0.10 | 2.0 | 0.39 | 0.31 | 1587 | 7595 | 1559 | 2.10 | <0.5 | 13.9 | 3.79 |
| | | 3 | 126 | 1.34 | 35658 | 2.23 | 3.5 | 1.83 | 3.93 | 1898 | 13752 | 1974 | 3.85 | 13.0 | 26.8 | 8.65 |
| | | 4 | 26593 | 130 | 0 | 0 | 7.6 | 60.5 | 14.2 | 15513 | 10171 | 0 | 41.8 | 13.7 | 25 | 53 |
| 7 | 600.92 | 1 | 21.0 | 11.5 | 43867 | 0.12 | 6.5 | 0.37 | 2.13 | 1440 | 18235 | 4140 | 15.7 | <0.5 | 69.2 | 10.2 |
| | | 2 | 35.8 | 5.99 | 31061 | <0.10 | 1.8 | 0.36 | 0.52 | 1579 | 7867 | 1519 | 2.53 | 0.60 | 14.6 | 4.10 |
| | | 3 | 167 | 1.63 | 33151 | 2.08 | 4.0 | 1.76 | 3.81 | 1896 | 12858 | 1895 | 4.01 | 12.7 | 25.5 | 7.83 |
| | | 4 | 26576 | 125 | 0 | 0 | 6.8 | 60.5 | 16.1 | 15885 | 10123 | 0 | 33.1 | 13.6 | 20 | 50 |
| 6 | 601.00 | 1 | 28.9 | 1.61 | 44564 | 0.13 | 7.1 | 0.25 | 1.79 | 1647 | 18678 | 4174 | 6.83 | <0.5 | 68.0 | 9.13 |
| | | 2 | 22.9 | 1.03 | 28729 | <0.10 | 1.9 | 0.26 | <0.50 | 1505 | 7440 | 1395 | 2.00 | 0.81 | 12.8 | 3.44 |
| | | 3 | 107 | 0.98 | 37994 | 2.27 | 4.2 | 1.48 | 3.52 | 2012 | 14206 | 2096 | 3.87 | 10.0 | 27.8 | 8.21 |
| | | 4 | 26442 | 130 | 0 | 0 | 6.3 | 58.0 | 14.2 | 15637 | 9303 | 0 | 41.7 | 17.2 | 21 | 54 |
| 5 | 601.40 | 1 | 21.5 | 11.6 | 44064 | 0.14 | 7.0 | 0.47 | 2.56 | 1390 | 18427 | 3646 | 7.85 | <0.5 | 66.1 | 12.2 |
| | | 2 | 24.5 | 8.70 | 31946 | <0.10 | 2.2 | 0.21 | 0.35 | 1628 | 7929 | 1310 | 2.05 | <0.5 | 13.3 | 4.18 |
| | | 3 | 106 | 3.65 | 40432 | 2.46 | 4.3 | 1.17 | 4.06 | 2203 | 15379 | 1947 | 4.52 | 8.00 | 29.3 | 9.78 |
| | | 4 | 25148 | 119 | 0 | 0 | 8.3 | 55.1 | 14.0 | 16678 | 9762 | 137 | 39.5 | 11.4 | 23 | 48 |
| 4 | 601.45 | 1 | 26.6 | 1.60 | 45252 | 0.19 | 7.6 | 0.41 | 1.40 | 1887 | 18605 | 3680 | 5.87 | 0.68 | 58.9 | 9.3 |
| | | 2 | 30.1 | 1.48 | 30399 | <0.10 | 2.3 | 0.25 | 0.07 | 1837 | 7658 | 1341 | 2.19 | <0.5 | 13.1 | 4.0 |
| | | 3 | 117 | 0.80 | 43679 | 2.55 | 5.1 | 0.99 | 3.46 | 2451 | 16429 | 2143 | 5.17 | 9.13 | 30.8 | 10.7 |
| | | 4 | 24626 | 121 | 0 | 0 | 7.7 | 51.3 | 12.9 | 14825 | 10131 | 85 | 38.4 | 8.69 | 30 | 44 |
| 3 | 601.52 | 1 | 22.8 | 5.14 | 44116 | 0.12 | 6.6 | 0.46 | 2.24 | 1060 | 18176 | 3760 | 6.64 | 1.36 | 71.6 | 9.2 |
| | | 2 | 27.8 | 4.34 | 30034 | <0.10 | 1.8 | 0.25 | 0.99 | 1461 | 7942 | 1167 | 2.40 | <0.5 | 15.8 | 4.0 |
| | | 3 | 146 | 1.66 | 19910 | 1.42 | 2.1 | 0.85 | 3.27 | 1439 | 7998 | 758 | 2.31 | 6.88 | 15.5 | 22.0 |
| | | 4 | 29603 | 121 | 0 | 0 | 8.1 | 63.4 | 18.1 | 23339 | 8878 | 0 | 52.9 | 10.2 | 18 | 42 |
| 2 | 601.59 | 1 | 19.9 | 2.24 | 43299 | 0.12 | 5.9 | 0.11 | 1.55 | 1054 | 17960 | 3753 | 5.08 | <0.5 | 72.2 | 7.7 |
| | | 2 | 19.7 | 2.21 | 31600 | <0.10 | 1.5 | 0.41 | 0.52 | 1288 | 8309 | 1060 | 1.48 | <0.5 | 15.9 | 3.2 |
| | | 3 | 128 | 1.02 | 16531 | 1.16 | 1.3 | 0.97 | 2.49 | 1222 | 6792 | 563 | 1.64 | 4.71 | 12.8 | 9.4 |
| | | 4 | 30632 | 123 | 0 | 0 | 9.1 | 68.5 | 20.2 | 24336 | 8606 | 0 | 61.8 | 15.6 | 19 | 57.7 |
| 1 | 601.94 | 1 | 19.9 | 2.59 | 41363 | 0.58 | 40.4 | 0.27 | 217 | 239 | 16257 | 4126 | 34.8 | <0.5 | 71 | 36.0 |
| | | 2 | 42.9 | 2.15 | 45057 | <0.10 | 11.5 | 0.62 | 49 | 2771 | 9796 | 2692 | 15 | <0.5 | 21.4 | 9.6 |
| | | 3 | 171 | 1.09 | 34973 | 2.28 | 36.6 | 3.04 | 103 | 2439 | 13703 | 1812 | 60.8 | 14.2 | 32.2 | 19.7 |
| | | 4 | 26767 | 89.3 | 0 | 0 | 73.5 | 67.1 | 233 | 11252 | 11378 | 0 | 127 | 26.0 | 18 | 74 |

[a] 1=exchangeable adsorbed elements, carbonates, and carbonate bound elements. 2=easily reducible fraction (including Mn-oxides and co-precipitated elements). 3=oxidizeable phases, organic matter, and sulphides. 4=residual.

grey layer (Table 1). Kaolinite and chlorite show maximum values in the background sediments and decrease slightly in the dolomitic claystones (Table 1). The negative vertical correlation of the illite with smectite in the dolomitic claystones, especially in the lowermost section (Table 1), could be partly due to

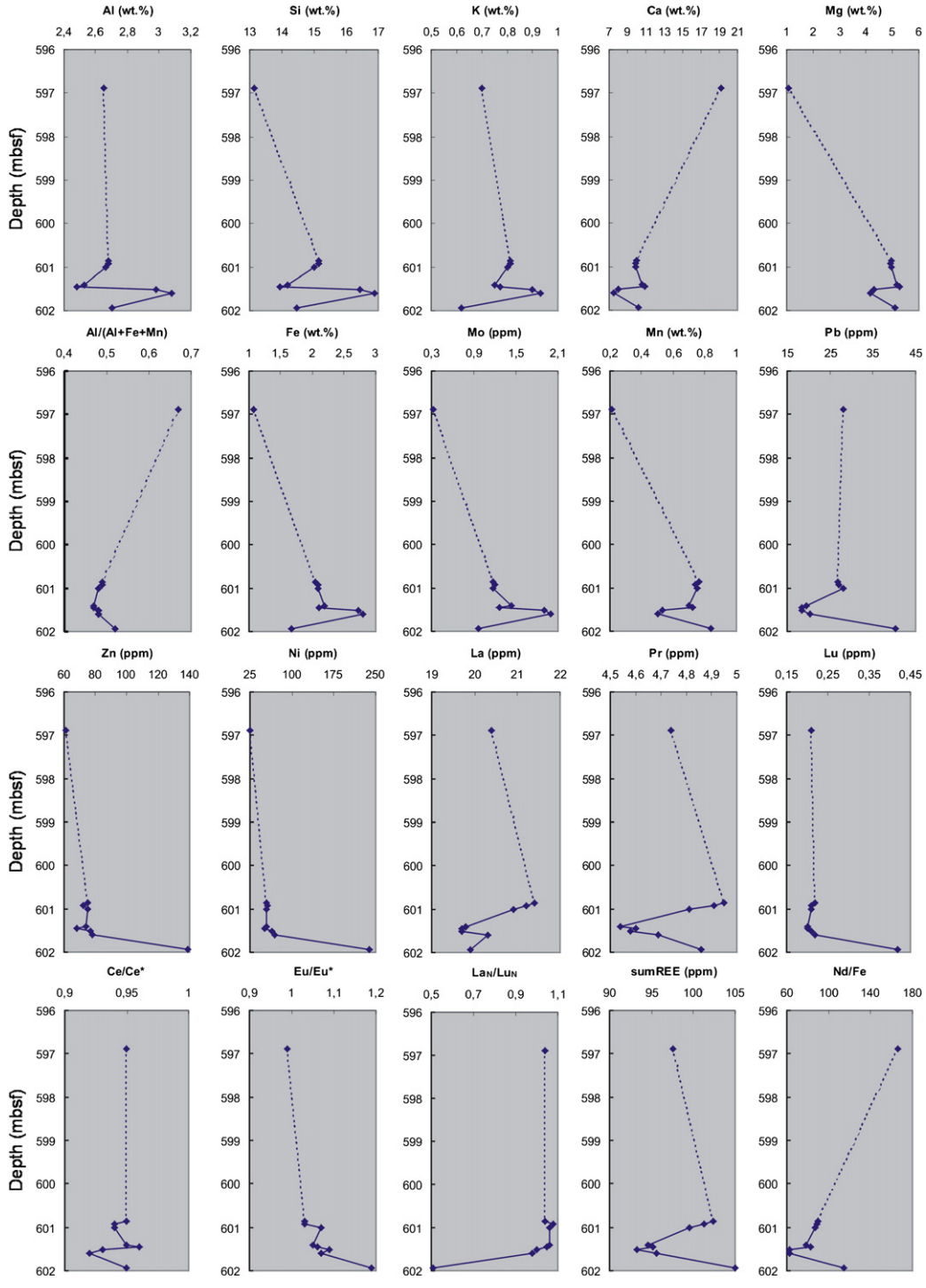


Fig. 5. Vertical distribution of selected elements and characteristic ratios along the lower dolomitic claystone section of ODP site 650 A.

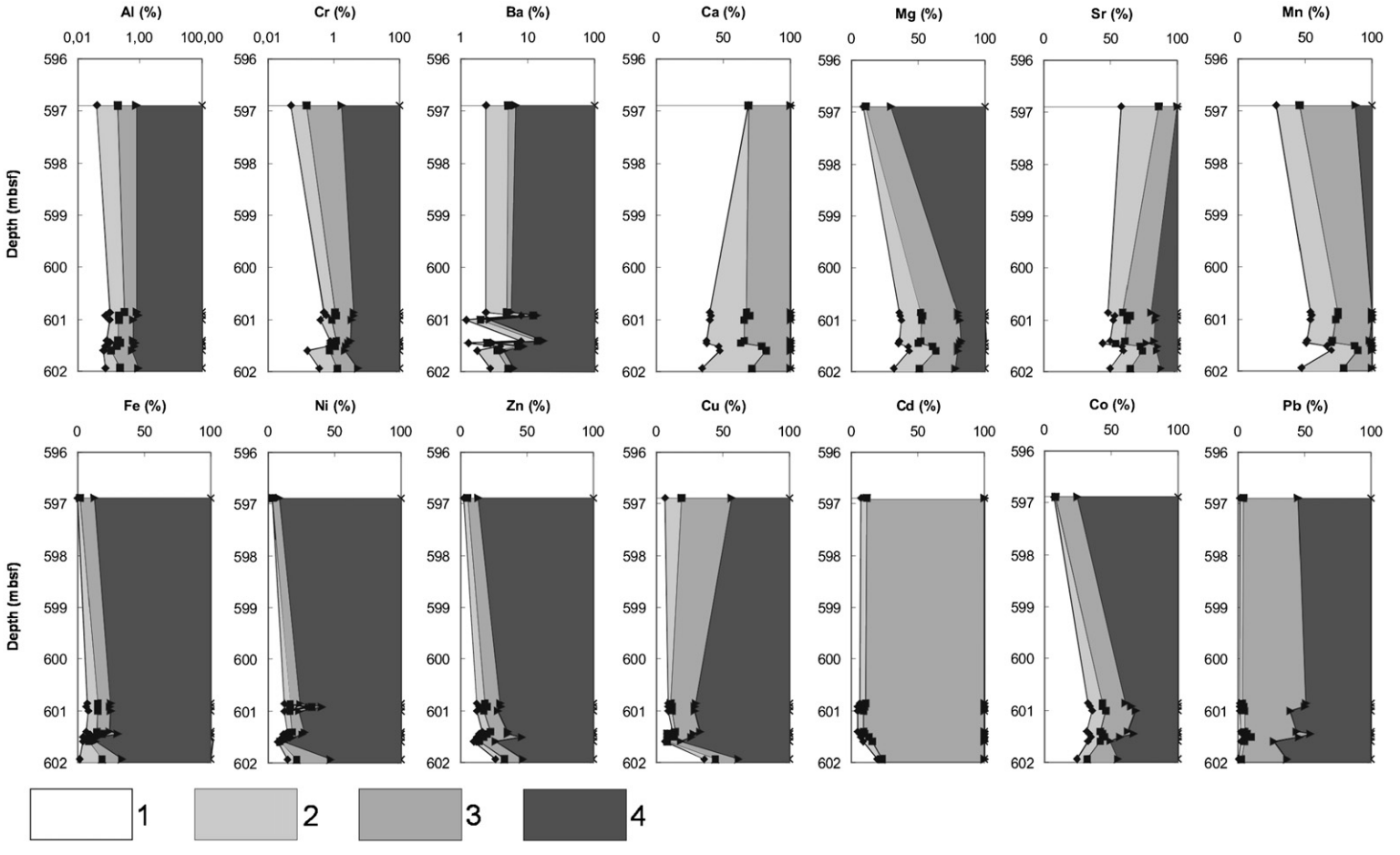


Fig. 6. Vertical phase distribution of selected elements along the lower dolomitic claystone section of ODP site 650 A: 1 = exchangeable adsorbed elements, carbonates, and carbonate bound elements; 2 = easily reducible fraction (including Mn-oxides and co-precipitated elements); 3 = oxidizeable phases, organic matter and sulphides; 4 = residual fraction.

dilution effect. The crystallinity of the two main clay minerals also varies along the vertical section. The progressive increase in the crystallinity of illite downward (Table 1; $n_{\alpha}$, according to Weaver, 1960) could be a diagenetic consequence. The crystallinity of smectite (montmorillonite) fluctuates with overall decrease upward in the section (Table 1; *V*/*p*, according to Biscaye, 1965). IR spectra (available on request) of all dolomitic claystone samples are identical and confirm the presence of the carbonates and silicates revealed by XRD.

### 4.2. Geochemistry

The dolomitic claystones show lower Ca and higher Mg, Fe, Mn, and Si concentrations than the overlying carbonate ooze (Table 2). Typical lithophile elements such as Al, Ti, Sn, Hf, Th, Zr, and Nb exhibit similar vertical distributions and are concentrated in the residual silicate fraction (Table 3; Figs 5 and 6). Silicon, as well as the alkaline elements (Li, Na, K, Rb, Cs) are also associated mainly with the lithogenic matter (Table 3, Fig. 5). Partitioning chemistry results (Fig. 6) show that more than 99% of Al is in the residual aluminosilicate phase and fluctuates negligibly along the core. Calcium and Sr are associated mainly with the carbonate fraction and correlated negatively with the lithogenic elements (Fig. 5). Whereas Ca is below detection limit in the residual fraction, some Sr is partitioned in it in the dolomitic claystone (Table 3, Fig. 6). Magnesium is mainly concentrated in the residual (aluminosilicate) fraction of the background sediments and in comparable proportions in the carbonate and aluminosilicate phases of the dolomitic claystone section (Fig. 6). Iron shows a vertical distribution much similar to those of the lithogenic elements (Table 3, Fig. 5). It is not only present in the lithogenic fraction, but occurs also in the oxyhydroxide–sulfide phases (phases 2 and 3; Fig. 6) in

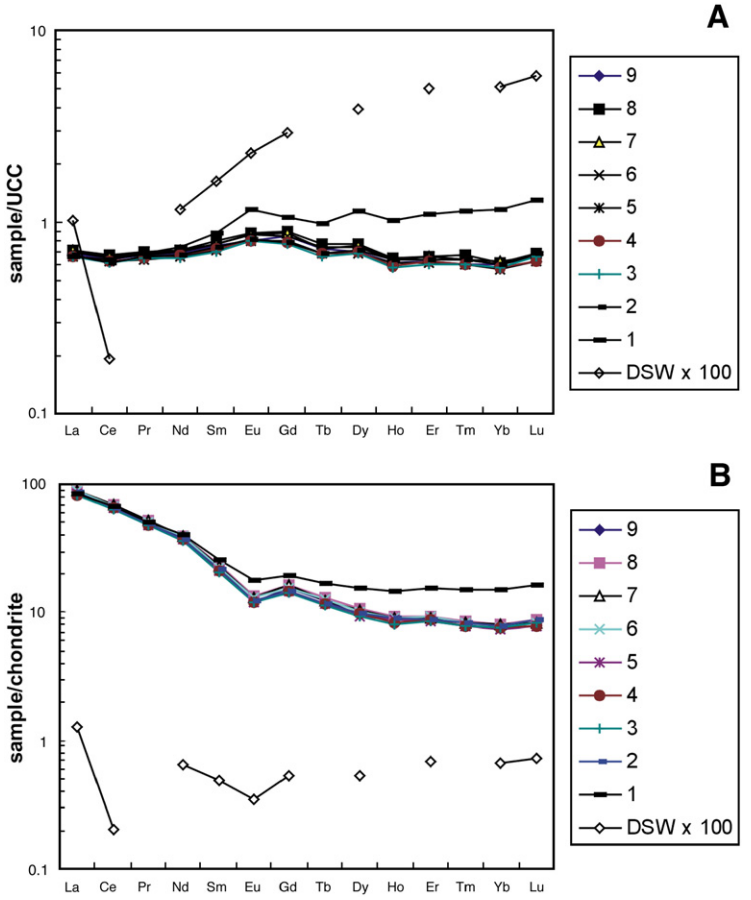


Fig. 7. (A) Upper continental crust-normalized (Taylor and McLennan, 1981) and (B) C1 chondrite-normalised (Sun and McDonough, 1989) REE distribution patterns for studied dolomitic claystone. Sample numbers see Table 1; DSW = western Mediterranean deep seawater (sample # 10708-2750 m; Greaves et al., 1991).

the lower and upper dolomitic claystone section. Vertical patterns comparable to that of Fe are shown also by Mo, P, Ga, and Ge. Manganese shows negative correlation with Fe ($r=-1.00$; Fig. 5) and is below detection limit in the aluminosilicate phase of the dolomitic claystones (Fig. 6). In the lower and upper part of the dolomitic claystone section, where it reaches maximum content, Mn is mainly in the carbonate and oxyhydroxide phases (Table 3, Fig. 6).

Trace elements can be divided into 4 groups according to their vertical distribution profiles. Lead, Tl, U, V, and Cr have similar vertical profiles and are enriched in the dolomitic claystones 2 to 6 times over the background values (Fig. 5). These elements can be hydrothermal (Pb, U, Tl) or hydrogenetic (Pb, U, Tl, V, Cr). Zinc, Cd, As, Sb, and Sc (enrichment 2 to 15 times over the background) also have identical vertical profiles (Fig. 5). Excluding Sc, a typical lithogenic element, the others from this group also can be either hydrothermal or hydrogenetic. The dolomitic claystones are 10 to 60 times enriched in Ni, Co, Cu, and Ta over the background values. These elements, hydrogenous and/or hydrothermal in nature, also show similar vertical distribution (Fig. 5).

Since the partitioning chemistry investigations imply a major terrigenous input (>40%) for most of the elements, we first normalized our REE data to the upper continental crust values. The REE distribution patterns (Fig. 7A) are overall sub-parallel, aligned close to 1.00, with almost no fractionation between LREE and HREE, and with a very weak negative Ce anomaly for some samples (Figs 5 and 7 A). C1 chondrite-normalized REE patterns of the dolomitic claystones show LREE enrichment, flat HREE distributions and negative Eu anomaly (Fig. 7 B).

### 4.3. Isotopic composition

Dolomitic claystone samples exhibit relatively small variations in their O and C isotopic compositions, ranging from 2.17 to 2.57 PDB $\delta^{13}C$ and 0.68 to 1.59 PDB $\delta^{18}O$ (Table 4). The nannofossil ooze sample, that overlays the dolomitic claystone sequence, has lower PDB $\delta^{13}C=0.6$ and PDB $\delta^{18}O=0.66$ values, compared to the dolomitic claystones (Table 4).

Strontium and Pb isotopic compositions (Table 4) were determined on totally digested samples, as well as

Table 4
Isotopic compositions of samples from the study area

| Sample # | Type[a] | $\delta^{13}C$ (‰)$_{PDB}$ | $\delta^{18}O$ (‰)$_{PDB}$ | $^{87}Sr/^{86}Sr$ | $^{206}Pb/^{204}Pb$ | $^{207}Pb/^{204}Pb$ | $^{208}Pb/^{204}Pb$ |
|---|---|---|---|---|---|---|---|
| M1-1 | Marsili basalt | – | – | – | 19.237 | 15.674 | 39.157 |
| M1-2 | Marsili basalt | – | – | – | 19.237 | 15.678 | 39.166 |
| M1-3 | Marsili basalt | – | – | – | 19.162 | 15.674 | 39.119 |
| M1-4 | Marsili basalt | – | – | – | 19.226 | 15.694 | 39.181 |
| M2-1 | Marsili basalt | – | – | – | 19.230 | 15.672 | 39.154 |
| V1-1691 | Marsili basalt | – | – | – | 19.277 | 15.687 | 39.218 |
| DSDP 373A | Vavilov basalt | – | – | – | 18.884 | 15.605 | 38.658 |
| 107–650A–65X–1 (50–53) | Sediment | 0.6 | 0.66 | 0.70949 | 18.863 | 15.672 | 38.939 |
| 107–650A–66X–1 (98–100) | Sediment | 2.17 | 0.78 | 0.71259 | 18.888 | 15.677 | 38.955 |
| 107–650A–66X–1 (104–106) | Sediment | 2.24 | 0.68 | 0.71258 | 18.888 | 15.680 | 38.959 |
| 107–650A–66X–1 (112–114) | Sediment | 2.36 | 0.92 | 0.71261 | 18.889 | 15.678 | 38.955 |
| 107–650A–66X–2 (2–4) | Sediment | 2.44 | 1.01 | 0.71232 | 18.869 | 15.670 | 38.926 |
| 107–650A–66X–2 (7–9) | Sediment | 2.51 | 1.02 | 0.71240 | 18.894 | 15.680 | 38.975 |
| 107–650A–66X–2 (14–16) | Sediment | 2.37 | 1.49 | 0.71247 | 18.889 | 15.676 | 38.950 |
| 107–650A–66X–2 (21–23) | Sediment | 2.33 | 1.54 | 0.71242 | 18.895 | 15.679 | 38.962 |
| 107–650A–66X–2 (56–59) | Sediment | 2.57 | 1.59 | 0.71115 | 18.891 | 15.669 | 38.938 |
| *Leaching experiments* | | | | | | | |
| 107–650A–65X–1 (50–53) | Phase 2[b] | – | – | – | 18.861 | 15.674 | 38.941 |
| 107–650A–66X–2 (14–16) | Phase 2 | – | – | – | 18.874 | 15.672 | 38.944 |
| 107–650A–66X–2 (56–59) | Phase 2 | – | – | – | 18.861 | 15.670 | 38.936 |
| 107–650A–65X–1 (50–53) | Phase 3 | – | – | – | 18.908 | 15.672 | 38.968 |
| 107–650A–66X–2 (14–16) | Phase 3 | – | – | – | 18.912 | 15.675 | 38.965 |
| 107–650A–66X–2 (56–59) | Phase 3 | – | – | – | 18.900 | 15.668 | 38.941 |
| 107–650A–65X–1 (50–53) | Phase 4 | – | – | 0.71955 | 18.906 | 15.690 | 39.018 |
| 107–650A–66X–2 (14–16) | Phase 4 | – | – | 0.71948 | 18.920 | 15.693 | 39.018 |
| 107–650A–66X–2 (56–59) | Phase 4 | – | – | 0.71972 | 18.905 | 15.685 | 38.995 |

[a] Basalt samples described in details in Savelli and Gasparatto, 1994.
[b] Phases as in Table 3.

on selected leachates and residues. $^{87}Sr/^{86}Sr$ ratios in the dolomitic claystones range from 0.71115 to 0.71261, values that are much more radiogenic than the present-day seawater. The carbonate ooze sample overlying the dolomitic claystones has $^{87}Sr/^{86}Sr = 0.70949$, which is much closer to seawater compared to the dolomitic claystone samples (Table 4).

## 5. Discussion

### 5.1. Mineralogy and geochemistry

Previous studies (McKenzie et al., 1990; Robertson, 1990) argued that the Marsili basal "dolostones" exhibit features similar to metalliferous sediments. Based on the widely used criteria for classification of metalliferous sediments ($Al/(Al+Fe+Mn) < 0.4$, Bonatti, 1981; or $(Fe+Mn)_{abiogenic} \geq 10$, Gurvich, 2006), neither our data (Table 2) nor data from the previous investigations confirm that the "dolostones" are metalliferous (ferruginous). The latter, however, does not exclude a weak hydrothermal influence in the basal dolomitic claystones. An alternative mode of hydrothermal influence to the previously proposed metasomatic model of McKenzie et al. (1990) is co-deposition of hydrothermal matter from hydrothermal plumes. It can be either low-temperature emanations forming primary Fe–Mn-oxyhydroxides, or "black smoker" sulfide–sulphate suspension within the background sediment. In such scenario the dolomitization would not be triggered by the hydrothermal processes.

In general, the metasomatic alteration hypothesis supposes gradual changes in the characteristics of the influenced rocks. The basal dolomitic claystones are homogenous and show no macroscopic features of gradual metasomatic influence. The mole fraction of $MgCO_3$ and the degree of order of the dolomite crystal lattice do not show any gradual changes upwards (Table 1). Fe- and Mn-oxyhydroxides content is below 4% (XRD detection limit). The content and degree of crystallinity of the other 2 main minerals, smectite and illite, show vertical changes. However, it is not clear if this is a result of metasomatic influence, diagenesis, or simply fluctuation in the primary alumino-silicate input from land. There are several general features in the elemental vertical distribution in the dolomitic claystones. Most of the elements (Cr, Ba, Ni, Zn, Cu, Co, Pb, excluding Cd) are mainly present in the residual aluminosilicate (sulfate for Ba) phase (Fig. 6). The common contribution of adsorbed, co-precipitated, oxyhydroxide, and sulfide phases to the content of the above elements is enhanced in the lower and upper dolomitic claystone parts (Fig. 6). Their maximum contents are in the basal greenish gray layer overlaying the basaltic basement (lowermost sample, Fig. 5). Submarine hydrothermal systems are major sources for the seawater of Li, Rb, Mn, Fe, and Si, and sinks for Mg and S (Von Damm, 1990). In general, Fe, Mn, Zn, Pb, and Cu are super-enriched in the hydrothermal solutions (Von Damm, 1990) and should have been contributed to the dolomitic claystones from the underlying basalts in view of the metasomatic hypothesis for the origin of the dolomites. On the other hand, the concentrations of these elements in the hydrothermal solutions respond systematically to changes in temperature (Seewald and Seyfried, 1990). Cooling can have a significant influence on the metal load of the hydrothermal fluids (Bowers et al., 1988). If we assume tepid solutions ($T < 70$ °C) derived from the basement as a dolomitizing agent for the basal carbonates (McKenzie et al., 1990), then we have to assume also that they carried a small metallic load. In this case, the non-lithogenic part of these elements might have been rather hydrothermally precipitated from jetting around hydrothermal springs or hydrogenous enrichment than injected from the basement as tepid solutions. Aluminium, Ti, Hf, Th, Zr, and Nb are immobile under low-temperature (tepid) hydrothermal conditions and should be mainly terrigenous in the dolomitic claystones. The similarity of the vertical distribution of Fe, presumably the main element contributed hydrothermally to the basal sediment, with those of the lithogenic elements (Fig. 5) indicates that Fe is mostly in the aluminosilicate fraction and argues against major hydrothermal input. Its presence in the oxyhydroxide-sulfide phases in some parts of the studied section (Fig. 6) can be interpreted to be either a possible weak hydrothermal influence or hydrogenous contribution. The vertical and phase distribution of Mn, another element that can be considered to be mainly of hydrothermal origin, suggests that even though it does not form XRD detectable mono or mixed Mn carbonates, a considerable part of Mn is in the Mg–Ca carbonate crystal lattice. This could be a result of either metasomatism by hydrothermal solutions, or diagenetic transformations during aging.

REE vertical profiles and distribution patterns also suggest mainly a lithogenic supply to the dolomitic claystones with a possible weak hydrothermal or hydrogenous signal. The very weak negative Ce anomaly implies negligible seawater influence on the dolomitic claystones' REE content (Figs 5 and 7 A). The middle dolomitic claystone part that is richest in lithogenic matter, is the most depleted in REE sediment (sumREE, Nd/Fe, Fig. 5). The noticeable difference of the REE signature of the lowermost sample from that of the

others with its slight positive Eu anomaly and distinct fractionation between LREE and HREE, (Figs 5 and 7 A) indicates either aeolian or weak hydrothermal input (e.g., Elderfield, 1988), or strong reducing conditions (McLennan, 1989), or presence of detrital feldspar (e.g., Murray et al., 1991). The feldspars are rare in all of the studied samples (Table 1) and we have no indications for strong reducing conditions throughout the sediment sequence ($C_{org}$, Table 1). The relatively enhanced contents of elements like Ni, Co, Cu, V, Zn, Cd, REE, and sumREE in the basal greenish gray layer are not typical for distal hydrothermal sediments and are compatible with hydrogenous enrichment of these elements. All this suggests rather a terrigenous than hydrothermal source for the observed REE pattern of the basal layer. The conversion of the positive Eu (upper continental crust normalization) into negative Eu (C1 chondrite normalization) anomaly is a well-known consequence of the normalization (e.g., Hekinian et al., 1993). Chondrite-normalized REE distribution patterns of the submarine low-temperature hydrothermal deposits are characterized by strong negative Ce anomaly, negative Eu anomaly, enrichment of LREE relative to HREE and very low total REE abundances (Marchig et al., 1982; Hekinian et al., 1993; Usui et al., 1997). Low-temperature hydrothermal influence to the studied sediments (e.g., McKenzie et al., 1990; Robertson, 1990) will mean phase precipitation (at least partial) in equilibrium with seawater. The immediate consequence of this will be a distinctive Ce depletion (similar to that in seawater) in the precipitated minerals, which is not observed (Fig. 7 B). The similarity of the dolomitic claystone REE patterns to those of exposed upper continental crust, sedimentary rocks, and post-Archean Australian shales (McLennan, 1989) with absolute abundances ranging from about 100x chondritic for La to 10–20× chondritic for Lu, LREE enrichment, flat HREE patterns and negative Eu anomalies with Eu/Eu* about 0.65–0.75 suggest terrigenous source of the REE to the sediments. The carbonate component of the studied sediments contributes negligibly to the REE patterns since the marine carbonates have substantially lower total REE abundances than the siliciclastic sediments (e.g., McLennan, 1989). Dolomitization of carbonates does not affect their REE patterns (Banner et al., 1988).

Overall, the above data indicate mainly lithogenic control of the trace element geochemistry of the basal dolomitic claystones. The enhanced concentrations of trace elements in the base of the dolomitic claystones could be a diagenetic consequence due to elemental exchange through the sediment–basalt interface at ambient temperatures during the basalt weathering and sediment diagenesis. However, no evidence of significant exchange is observed in the isotopic composition of the basal layer, as will be discussed below. Therefore, the enhanced concentrations most probably reflect low carbonate sedimentation rates and subsequently prolonged scavenging of trace metals by Mn–Fe-oxyhydroxides from the seawater.

We have no direct determinations of the age of the basal dolomitic claystones and can infer it from the age of the underlying basaltic basement. Paleontological and paleomagnetic data suggest that the age of the Marsili Basin basement is upper Pliocene (~2 Ma) (Kastens et al., 1987), indicating that the age of the studied dolomitic claystones is also around 2 Ma. The glacial value of $\delta^{18}O$ recorded at 2.03 Ma (Nebout and Grazzini, 1991) suggests that the Marsili basal oozes were formed during a glacial stage. During that time the seasonal contrast increased and the summer dryness extended to the whole Mediterranean area. In general, the accumulation rate of the terrigenous fraction is higher during glacial stages as a result of drier continental climate, reduced vegetation cover, increased wind strength, and erosion from exposed shelf areas due to lower sea level stands (Rea, 1994). During glacial stages the tropical arid areas had 5 times larger extend, wind speeds were 1.3–1.6 times higher, and Fe-rich atmospheric dust loads were 10–20 times greater than during interglacial stages (Sarnthein, 1978; Petit et al., 1981; De Angelis et al., 1987; Martin, 1990). Terrigenous input in the western Mediterranean Sea correlates with glacial/interglacial cycles (Hoogakker et al., 2004). It increases during glacial periods as a result of drier and colder climate in the source areas and more frequent and intense outbreaks of dust transport. The colder and drier climatic conditions in combination with low sea level allow rivers to discharge their sediment load closer to the shelf edge, promoting enhanced fluvial input into the basin. Saharan dust blown out from North Africa is the major source of natural aerosols over the Mediterranean (Guerzoni and Chester, 1996). It is characterized by high Al, Si, Ca, Mg, Fe and Mn concentrations (Guerzoni et al., 1989). The eolian transport of Saharan aerosols is responsible for the episodes of "red snow" or "red rain" in Europe (Pye, 1987). Few episodes of "red rains" account for more than 50% of the recent total annual particle flux to the Mediterranean (Löye-Pilot et al., 1986). An estimate (Correggiari et al., 1989) of the relative contribution of elements from the rivers and atmosphere indicates that the atmospheric deposition accounts for 25–50% of the recent total terrigenous input in the Tyrrhenian Sea. Another mode of terrigenous supply to the Marsili Basin is through turbidity currents

(Hieke et al., 1990), composed of land-derived, volcaniclastic and biogenic components. Tremors released by volcanic activity, tectonic movements as well as sea-level changes may have acted as triggering events for the turbidity currents. Apparently the precursor of the studied dolomitic claystones, nannofossil oozes, formed at the commencement of opening of the Marsili Basin. This event (~2 Ma) coincided with the consecutive glaciation. It is highly possible that glacially induced high terrigenous influx (eolian and/or fluvial) to the Tyrrhenian Sea led to the formation of brightly coloured calcareous–terrigenous basal sediments, which were the precursor of the dolomitic claystones.

### 5.2. Isotopic composition

#### 5.2.1. Oxygen and carbon isotopes

Comparison between dolomitic claystones recovered from ODP Site 650 and Site 651 (Vavilov Basin) reveals that there is positive correlation between O and C isotopic compositions with two distinct trends (Fig. 8). Regression lines fitted through the trends exhibit slopes around 0.6 and 0.3 respectively. The slope of 0.3 is relatively close to the slope of 0.25 expected for variations produced as a result of only temperature variations during dolomitization. However, majority of the samples plot within the steeper trend that cannot be explained by only variations in the temperature. Several alternative hypotheses can be explored for the origin of the steeper trend. It is possible that the isotopic variations in the Site 650 and 651 dolomitic claystones were inherited from the proto-carbonate substrate, or reflect diagenetic changes, or two or more solutions with distinct isotopic compositions were involved in the dolomitization. McKenzie et al. (1990) proposed that the two end-member solutions, involved in the dolomitization of the sediments at Site 651 could have been the ambient seawater and a seawater fluid, modified during a reaction with the underlying basalts. Site 650 O and C isotopic data plot in the middle of the Site 651 steeper trend (Fig. 8), indicating that similar processes may have been involved in their genesis. Present-day Mediterranean seawater has $\delta^{18}O$ around 1‰ SMOW (Vergnaud-Grazzini, 1985) and 9 of the analyzed 10 pore-water samples from Site 651 show values between 1‰ and 1.7‰ SMOW (McKenzie et al., 1990). Therefore, assuming precipitation from fluids with $\delta^{18}O$ 1‰ and 1.5‰ SMOW, temperatures between 26 °C and 32 °C respectively, can be calculated for the formation of the Site 650 dolomitic claystones, using water-dolomite fractionation equation of Matthews and Katz (1977): $10^3 \ln\alpha = 3.06 \times 10^6 T^{-2} - 3.24$. These calculations are in agreement with the precipitation temperatures between 14 °C and 44 °C, calculated by McKenzie et al. (1990) for the Site 651 dolomites. At present, the temperature of the ambient seawater is around 13–14 °C. Therefore, the calculated formation temperatures by McKenzie et al. (1990) would be in agreement with two possible fluid end-members with different temperatures: one being ambient seawater, and another one being heated seawater. Tepid seawater fluid, however, would probably have more or less similar O isotopic composition to the ambient seawater. Then, the trend on $\delta^{13}C$ vs $\delta^{18}O$ plot will be expected to be close to 0.25, i.e. the isotopic variation will be solely a result of temperature changes, which is not the case for most of the samples (Fig. 8). Therefore, alternative explanations for the positive correlation between the O and C isotopic compositions can be isotopic variations in the proto-carbonate and/or diagenetic changes (e.g., Aloisi et al., 2000). Marine carbonates inherit their oxygen isotopic composition from the seawater. The possibility for arid climatic conditions during the initial opening stage of the Marsili Basin will contribute to enhanced evaporation at the surface and subsequently to formation of carbonates with elevated $\delta^{18}O$. Therefore, the trend toward more positive $\delta^{18}O$ values can be explained by precipitation from $^{18}O$-enriched water. Mixing of $^{18}O$-enriched surface seawater with lighter seawater and/or meteoric fluid will generate carbonates, including dolomites with positive correlation between $\delta^{13}C$ vs $\delta^{18}O$ (Mayers et al., 1997). Alternatively, it is possible that the dolomitic claystones were affected to some degree by diagenetic processes. Dehydration of clay

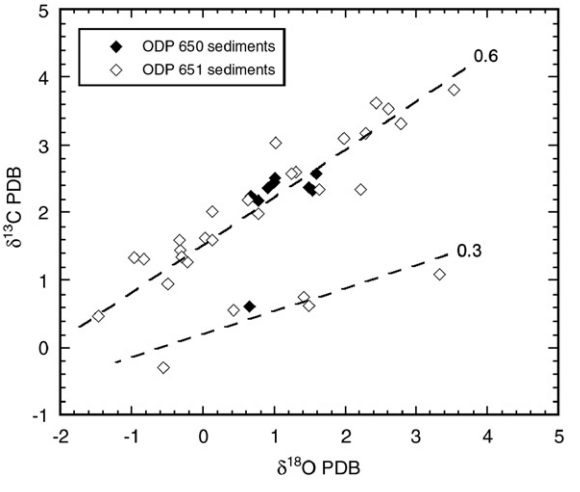


Fig. 8. Comparison of oxygen and carbon isotopic compositions of ODP 650 and 651 basal dolomitic claystones. 0.6 and 0.3 are the approximate slopes of the 2 trends formed by the data. Site 651 data from McKenzie et al. (1990).

minerals can produce pore waters with increased $\delta^{18}O$ values (e.g., Aloisi et al., 2000). Interaction of such $^{18}O$-rich diagenetic fluid with the carbonates will also result in elevated $\delta^{18}O$ in the dolomitic claystones in both Marsili and Vavilov basins.

*5.2.2. Strontium and lead isotopes*

The elevated Sr isotopic compositions of the dolomitic claystones and nannofossil ooze are a result of incorporation of lithogenic material in the sediments. Essentially, the Sr isotopic compositions of the totally digested dolomitic claystone and carbonate samples represent mixtures of less radiogenic, most probably seawater-derived Sr and more radiogenic Sr from the lithogenic fraction. The residues have almost identical $^{87}Sr/^{86}Sr$ ratios, ranging between 0.7195 and 0.7197, more radiogenic than the bulk dolomitic claystones and carbonate ooze sample (Fig. 9). The Sr isotopic composition of the residues reflects the composition of the lithogenic fraction, which itself may be used to trace the source of the terrigenous input to the sediments. Overall, the radiogenic nature of the dolomitic claystones and the residues argues against significant contribution of Sr from the Aeolian Arc or Marsilli Seamount, both characterized by relatively non-radiogenic Sr isotopic compositions, around 0.704–0.707 (Beccaluva et al., 1990; De Astis et al., 2000; Calanchi et al., 2002). Another possible Sr source for the sediments in the area is dust material transported from North Africa. The Sr isotopic composition of the Saharan dust overall decreases from west to east, with $^{87}Sr/^{86}Sr$ between 0.7193 and 0.7245 measured in Corsica (Grousset et al., 1998) and between 0.7160 and 0.7192 measured in the eastern Mediterranean (Krom et al., 1999). The Sr isotopic composition of the residues overlaps with the most and least radiogenic compositions of the eastern and western Mediterranean Saharan dust, respectively. Geographically ODP Site 650 is close to Corsica, therefore, it is plausible that the western Mediterranean component is the likely contributor of Sr to the basal sediments in the Marsili Basin. Overall, the average Sr isotopic composition (around 0.722) of the western Mediterranean Saharan dust is slightly more radiogenic than the residues, which may be a result of small contribution to the terrigenous fraction of less radiogenic Sr from a source similar to the nearby Aeolian Arc volcanoes (Fig. 9). The volcanism in the Aeolian Arc began around 1 Ma ago (e.g., Francalanci and Manetti, 1994), which postdates the dolomitization event by at least several hundred thousand to a million years. Although the present-day Aeolian Arc probably did not exist during the very early stages of the development of the Marsili Basin, an older, Pliocene arc existed in the region (Savelli, 1988) that possibly supplied material to the newly forming basin.

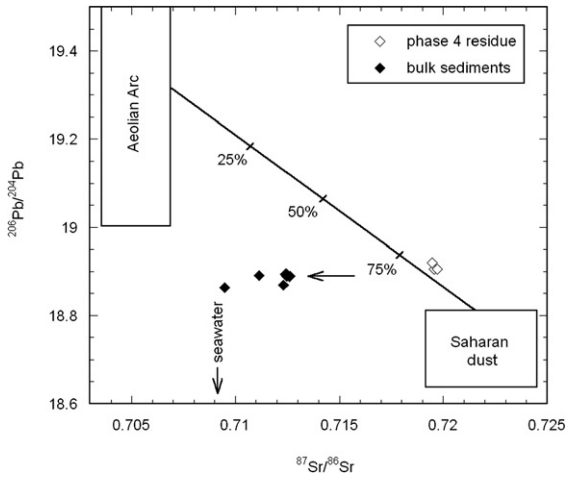


Fig. 9. $^{206}Pb/^{204}Pb$ vs $^{87}Sr/^{86}Sr$ of bulk sediments and residues compared to Aeolian Arc volcanoes and Saharan dust. The bulk sediments require addition of Sr from the seawater to explain their $^{87}Sr/^{86}Sr$ composition. Note that the isotopic composition of the residues can be modeled by mixing between Saharan dust and Aeolian Arc volcanoes. Although the present-day Aeolian Arc is younger than the basal sediments at ODP site 650, there are data indicating existence of Pliocene arc in the region, for more discussion see the text. Saharan dust field includes data for North Africa granitoids, data from Juteau et al. (1986), Hamelin et al. (1989), and Krom et al. (1999). Aeolian Arc volcanoes data from compilation in Francalanci and Manetti (1994), De Astis et al. (2000), and Calanchi et al. (2002).

Lead in the Mediterranean region can be derived from Saharan dust and from volcanic and crustal sources in the region (e.g., Abouchami et al., 1999). In addition to the Mediterranean area, most of the pre-industrial Pb in the north-central Atlantic sediments was also contributed from Saharan dust during the last several million years (Hamelin et al., 1989; Abouchami et al., 1999). The Pb isotopic composition of the pre-Holocene Atlantic sediments is controlled mainly by mixing of Saharan dust and seawater Pb (Hamelin et al., 1989; Abouchami and Zabel, 2003). Overall, our data plot entirely within the field of the pre-Holocene Atlantic sediments (Fig. 10), suggesting that the Pb in ODP Site 650 sediments can also be controlled by Saharan dust and seawater. Lead isotopic data for the Mediterranean seawater, however, exhibit $^{206}Pb/^{204}Pb$ ratios between 18.7 and 18.78 (Abouchami et al., 1999) and overlap with the Saharan dust composition (Fig. 10). The composition of the dolomitic claystones, therefore, cannot be explained simply by mixing of Saharan dust and Mediterranean seawater Pb. High-precision Pb isotopic analyses on leachates, residues, and

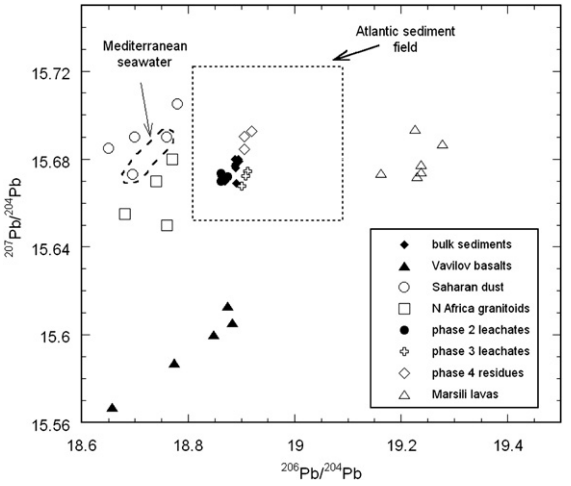


Fig. 10. Comparison of Pb isotopic compositions of ODP site 650 dolomitic claystones, leachates and residues with Saharan dust, Marsilli and Vavilov lavas and Mediterranean seawater. Saharan dust and North Africa granitoids data from Juteau et al. (1986) and Hamelin et al. (1989), Vavilov lavas from Hamelin et al. (1979), and Mediterranean seawater from Abouchami et al. (1999).

bulk sediments revealed some minor variations in the different components that built the sediments. The phase 2 leachates have slightly less radiogenic Pb compared to the bulk sediments, which may be a result of some seawater Pb incorporation (Fig. 10). Overall, however, their composition is very close to the bulk dolomitic claystones. Similarly, phase 3 leachates and the residues are also very close to the bulk dolomitic claystones (Fig. 10), which suggest that the Pb in the Site 650 is controlled mainly by the terrigenous input in the region (Fig. 10). Alternative explanation for the relative isotopic homogeneity in the Pb isotopic composition of the Site 650 sediments can be that the different phases represented by the leachates and residues equilibrated during the dolomitization event. The composition of the nannofossil ooze, as well as the preserved heterogeneity in the Sr isotopic compositions between whole-rocks and residues (Table 4), however, argue against complete homogenisation during dolomitization.

Most probably the Pb in the sediments simply reflects contribution from the African continent (i.e. Saharan dust) and source with isotopic characteristics similar to the Aeolian Arc volcanoes, possibly the Pliocene arc that existed in the region. Simple mixing between Saharan dust and Aeolian Arc volcanic material can explain the Pb and Sr isotopic composition of the terrigenous fraction of Site 650 sediments (Fig. 9). Overall, more than 75–80% of the Pb and Sr in the terrigenous phase of the sediments were contributed by Saharan dust (Fig. 9).

### *5.2.3. Hydrothermal leaching of basalts versus seawater contribution of $Mg^{2+}$ for the dolomitization*

An alternative hypothesis that must be addressed is hydrothermal input of material to the sediments, because hydrothermal circulation through the basalts will scavenge Pb and Sr from the Marsili basal lavas and mixing it with material with Saharan origin will also result in isotopic characteristics similar to those of the dolomitic claystones. The lithogenic fraction of the background ooze sample, however, has very similar Sr and Pb isotopic composition to the dolomitic claystones. There is no reason to believe that any hydrothermal circulation was still active at the time of the ooze deposition, indicating that Sr and Pb were controlled by the terrigenous input to the basin. In addition, leaching experiments failed to reveal Pb with distinct isotopic compositions in the different fractions that make up the dolostones and carbonate ooze (Fig. 10). Later indicating that even if there was hydrothermal activity during dolomitization, it did not contribute significant amount of Pb and possibly metals that share similar geochemical behaviour such as Zn, Cu, and Ag to the hydrothermal/hydrogenous fraction of the sediments. It is evident from our isotope data that the input sources to the ODP Site 650 sediments did not change during and after the dolomitization event, arguing against any significant hydrothermal contribution of metals, including Mg. Basement rocks of Hole 650 are altered vesicular basalts with low MgO abundance (1.93–3.93 wt.%) interpreted as Mg depletion due to basalt/seawater interaction at low temperature under oxidising conditions (Beccaluva et al., 1990). One might be tempted to speculate that the solutions resulted from such an interaction will be Mg-rich and capable to dolomitize the overlaying 2-meter sediment sequence. However, the basement at Site 651 (Vavilov Basin) has 2–3 times more MgO that the Site 650 basalts (6.53–8.42 wt.%), but is overlain by 40 m thick dolomitic claystone sequence (Beccaluva et al., 1990). Apparently, there is no correlation between the Mg content and the dolomitization, suggesting that the latter is not linked to the basement alteration.

The unusual geochemistry of the hydrothermal vents at the Kasuga Seamounts (Northern Mariana Arc) indicates that at specific conditions low-temperature hydrothermal fluids might be enriched in $Mg^{2+}$, $SO_4^{2-}$, Si, $Fe^{2+}$, $Mn^{2+}$, $Ba^{2+}$, B, $Li^{+}$, $Rb^{+}$and depleted in $Ca^{2+}$over ambient seawater (McMurtry et al., 1993). The calculations suggest that the warm fluid (~40 °C) is close to saturation with respect to dolomite, which may control the $Mg^{2+}$and $Ca^{2+}$ concentrations in the fluid below the seafloor (McMurtry et al., 1993). The Kasuga Seamount fluids deposit nontronite and Fe- and Mn-oxyhydroxides at the summit, however, none of these phases were found in the Marsili

dolomitic claystones. It is possible that fluids, highly enriched in Si, precipitated as montmorillonite instead of nontronite as is the case at the Kasuga Seamount. However, still speculative remains the scale of dolomitization, which obviously was widespread at large areas in the Marsili and Vavilov Basins. The discharge of Mg-rich warm fluids at Kasuga Seamount is focused (McMurtry et al., 1993) while at the Marsili and Vavilov Basins case very large-scale diffusive discharge through a carbonate blanket is required. The newly discovered class of serpentinite-hosted sea-floor hydrothermal systems (e.g., the Lost City) emanates Mg-rich, low-temperature (<90 °C), high-pH (9–11), methane- and hydrogen-rich fluids which precipitate carbonates ($CaCO_3$) and hydroxides ($Mg(OH)_2$) upon mixing with seawater (Kelley et al., 2001, 2002; Früh-Green et al., 2003; Kelley et al., 2005). The features of these fluids (Mg-rich, low-temperature, carbonate precipitation) raise again the question of possible hydrothermal origin of the ODP Site 650 dolomitic claystones. However, a zero-Mg end member fluid is produced in the serpentinization reaction zone of the Lost City field (Kelley et al., 2005). The primary precipitates are aragonite and brucite, but the brucite is a later phase formed through mixing of Mg-rich seawater and hydrothermal fluid. Aragonite converts to calcite through time and brucite dissolves away as it is undersaturated in seawater (Früh-Green et al., 2003; Kelley et al., 2005). No dolomite has been found in these giant hydrothermal carbonate deposits.

### 5.3. Dolomite formation model

A number of models involving seawater alone as a source for Mg for marine dolomitization have been proposed (Tucker and Wright, 1990). With little modification, seawater itself may be able to dolomitize if there is an efficient mechanism to pump it through carbonate sediments (Land, 1985). Driving mechanism for such pumping process might be high heat flow through the basement, which produces thermal convection of pore waters in the sediment. This could be a major dolomitization mechanism since it provides a means of transporting very large volumes of seawater through the sediment. Based on the geologic context of the region we suggest the following model of dolomitization of the Marsili basal calcareous sediment (Fig. 11). The conductively cooling thin young lithosphere, generated by diffuse spreading and dyke emplacement, produces high heat flow. This causes low-temperature passive convection of the pore waters in the basal sediment. In addition, the convection is enhanced in response to density gradients between seawater with elevated salinity due to evaporation (a result of the arid climatic conditions during the glacial

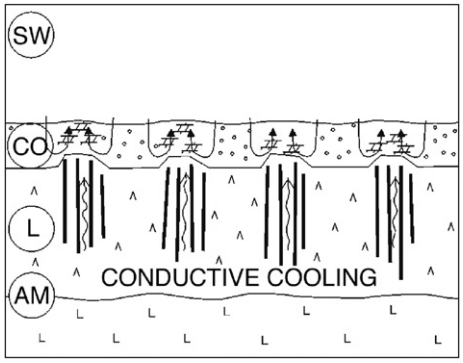


Fig. 11. Dolomitization model based on seawater (SW) circulation through the calcareous oozes (CO) caused by convection driven by passive conductive cooling of thin new oceanic lithosphere (L); diffuse spreading with dyke emplacement, and shallow asthenospheric mirror (AM).

stage) and geothermally-heated porewaters within the sediment. The dense seawater is drawn into the sediment displacing the less dense porewaters. The combination of basement topography and sediment thickness variations controls the sites of recharge and discharge, with high heat flow and upflow occurring at basement highs and downflow at basement lows (e.g., Alt, 1995). Much of this circulation may occur at discrete permeability zones and the dolomitization will have patchy distribution (e.g., at Sites 650 and 651, but not at Site 655).

The proposed mechanism will invoke the question why there are no dolomite layers in the basal carbonate oozes on the mid-ocean ridge (MOR) flanks, where low-temperature seawater convection is also occurring. At the MOR flanks, away from the axial zone, the heat source is the cooling plate and this drives seawater convection cells, but they are shallow, weak and probably not powerful enough to dolomitise the calcareous sediment. At the onset of opening of the Marsili Basin there was probably diffuse spreading throughout the small back-arc basin which supplied very high heath flow that was able to drive large seawater masses through the thin calcareous sediment. The possible weak hydrothermal signal deduced from the Fe and Mn forms of presence and content, as well as the alteration and Mg-depletion of the fractured portions of igneous basement suggest that we cannot fully exclude a seawater circulation through the uppermost levels of basement. Presented data, however, indicate that the dolomitization most probably was not related to the basalt alteration, but to complex climato-tectonic changes that occurred during the early stages of basin opening.

## 6. Summary

Detailed geochemical study reveals that the red–brown dolomitic claystones at ODP Site 650 do not

exhibit features of gradual metasomatic influence, suggesting that hydrothermal leaching of the underlying basaltic sequences was not important for their formation, as considered previously (McKenzie et al., 1990; Robertson, 1990). The presence of most of the elements (excluding Ca, Mn, Cd, and to some extent Sr and Mg) mainly in the aluminosilicate (sulfate for Ba) phase suggests that the dolomitic claystone precursor was formed as a result of mixing of background carbonate and lithogenic matter. Slightly enhanced content of Fe, Cu, Zn, Pb, Ni, Co, Cd in the adsorbed, co-precipitated, oxyhydroxide, and sulfide phases in the lower and upper dolomitic claystone parts may indicate weak hydrothermal influence or enhanced hydrogeneous input. The more pronounced increase of Ni, Co, Cu, V, Zn, Cd, and REE, however, in the basal greenish gray layer is not typical for hydrothermal sediments and indicates hydrogenous imprint.

The Marsili basal sediment sequence was deposited in the early stages of the opening of the Marsili Basin. This event (~2 Ma) coincided with the consecutive glaciation. Positive $\delta^{13}C$ vs $\delta^{18}O$ correlation indicates that part of the isotopic variations in the dolomitic claystones can be attributed to temperature variations during the dolomitization. However, majority of the samples form a steeper trend that cannot be produced by only temperature variations, indicating that stable isotope characteristics were possibly inherited from the proto-carbonate. In addition, dehydration of clay minerals during diagenesis may also contribute elevated $\delta^{18}O$ to the dolostones. The glacially induced high terrigenous influx to the Tyrrhenian Sea contributed the other main component of the brightly coloured basal sediment (i.e., the clays). Strontium and Pb isotopic compositions provide evidence that the aluminosilicate fraction of the dolomitic claystones is controlled mainly by Saharan dust (75%–80%), plus some contribution from a source, similar to the Aeolian Arc volcanoes (20%–25%), most probably a Pliocene volcanic arc that existed in the region. No significant hydrothermal contribution of Pb and other metals with similar geochemical behaviour from the volcanic basement was detected, which furthermore argues against a hydrothermal metasomatic origin of the dolomitic claystones. Strontium and Pb isotopic compositions of the dolomitic claystones and the overlying non-dolomitized sediment are overall very similar, indicating that the metal input to the ODP Site 650 basal sediments was the same during and after dolomitization, which suggests that dolomitization was not related to hydrothermal event contributing Mg and other metals from the underlying basaltic basement. We suggest that the seawater alone was the Mg source dolomitizing the basal calcareous sediment. The conductively cooling new lithosphere produced high heat flow that was able to drive pore water convection and consequently large volumes of seawater could pass through the sediment. The combination of tectonic and climatic factors, including initial basin opening, arid climate, and high terrigenous influx lead to the formation of the basal red–brown dolomitic claystones.

## Acknowledgements

We express our gratitude to the ODP Program for providing the sample material. CNR-NATO grant (outreach fellowship program) to V. M. Dekov is gratefully acknowledged. We would like to thank J. Curtis for the assistance with the C and O isotope analyses. G. Kamenov was supported by University of Florida Alumni Fellowship and by NSF grant EAR-0418905 during the course of this work. We would like to thank E. Bonatti (IGM-CNR, Italy) for valuable hints during the progress of this work. Thanks go to G. Valdre (University of Bologna, Italy), V. Landuzzi, L. Langone (both from IGM-CNR, Italy), and J. Scholten (University of Kiel, Germany) for the XRD and organic C analyses. H. Chamley (Université Pierre et Marie Curie, France), R. Lenaz (IGM-CNR, Italy), J. McKenzie (ETH Zurich, Switzerland), and A. Robertson (University of Edinburgh, UK) provided important references. We are much indebted to G. J. De Lange, J. Compton and anonymous reviewer for the valuable suggestions, which substantially improved this manuscript.

## References

Abouchami, W., Zabel, M., 2003. Climate forcing of the Pb isotope record of terrigeneous input into the equatorial Atlantic. Earth Planet. Sci. Lett. 213, 221–234.

Abouchami, W., Galer, S.J., Koschinsky, A., 1999. Pb and Nd isotopes in NE Atlantic Fe–Mn crusts: proxies for trace metal paleosources and paleocean circulation. Geochim. Cosmochim. Acta 63, 1489–1505.

Aloisi, G., Pierre, C., Rouchy, J.M., Foucher, J.P., Woodside, J., the MEDINAUT Scientific Party, 2000. Methane-related authigenic carbonates of eastern Mediterranean Sea mud volcanoes and their possible relation to gas hydrate destabilisation. Earth Planet. Sci. Lett. 184, 321–338.

Alt, J.C., 1995. Subseafloor processes in mid-ocean ridge hydrothermal systems. In: Lupton, J., Mullineaux, L., Zierenberg, R. (Eds.), Seafloor Hydrothermal Systems: Physical, Chemical, Biological and Geological Interactions within Submarine Hydrothermal Systems. AGU Monograph, vol. 91, pp. 85–114.

Argnani, A., Savelli, C., 1999. Cenozoic volcanism and tectonics in the southern Tyrrhenian Sea: space-time distribution and geodynamic significance. J. Geodyn. 27, 409–432.

Banner, J.L., Hanson, G.N., Meyers, W.J., 1988. Rare earth element and Nd isotopic variations in regionally extensive dolomites from the Burlington–Keokuk Formation (Mississippian): implications

for REE mobility during carbonate diagenesis. J. Sediment. Petrol. 58, 415–432.

Beccaluva, L., Bonatti, E., Dupuy, C., Ferrara, G., Innocenti, F., Luchini, F., Macera, P., Petrini, R., Rossi, P.L., Serri, G., Seyler, M., Siena, F., 1990. Geochemistry and mineralogy of volcanic rocks from ODP sites 650, 651, 655, and 654 in the Tyrrhenian Sea. In: Kastens, K.A., Mascle, J., et al. (Eds.), Proc. ODP, Sci. Results, vol. 107, pp. 49–74.

Biscaye, P.E., 1965. Mineralogy and sedimentation of recent deep sea clays in the Atlantic Ocean and adjacent seas and oceans. Geol. Soc. Amer. Bull. 76, 803–832.

Bonatti, E., 1981. Metal deposits in the oceanic lithosphere. In: Emiliani, C. (Ed.), The Sea, vol. 7. John Willey and Sons, N.Y., pp. 639–686.

Bowers, T.S., Campbell, A.C., Measures, C.I., Spivack, A.J., Khadem, M., Edmond, J.M., 1988. Chemical controls on the composition of vent fluids at 11°–13°N and 21°N, East Pacific Rise. J. Geophys. Res. 93, 4522–4536.

Calanchi, N., Peccerillo, A., Tranne, C.A., Lucchini, F., Rossi, P.L., Kempton, P., Barbieri, M., Wu, T.W., 2002. Petrology and geochemistry of volcanic rocks from the island of Panarea: implications for mantle evolution beneath the Aeolian Island Arc (southern Tyrrhenian Sea). J. Volcan. Geotherm. Res. 115, 367–395.

Correggiari, A., Guerzoni, S., Lenaz, R., Quarantotto, G., Rampazzo, G., 1989. Dust deposition in the central Mediterranean (Tyrrhenian and Adriatic Seas): relationships with marine sediments and riverine input. Terra Nova 1, 549–558.

Davidson, C.M., Thomas, R.P., McVey, S.E., Perala, R., Littlejohn, U.D., 1994. Evaluation of a sequential extraction procedure for the speciation of heavy metals in sediments. Anal. Chim. Acta 291, 277–286.

De Angelis, M., Barkov, N.I., Petrov, V.N., 1987. Aerosol concentrations over the last climatic cycle (160 kyr) from an Antarctic ice core. Nature 325, 318–321.

De Astis, G., Peccerillo, A., Kempton, P.D., Volpe, L., Wu, T.W., 2000. Transition from calc–alkaline to potassium-rich magmatism in subduction environments: geochemical and Sr, Nd, Pb isotopic constraints from the island of Vulcano (Aeolian Arc). Contrib. Mineral. Petrol. 139, 684–703.

Dekov, V.M., Savelli, C., 2004. Hydrothermal activity in the SE Tyrrhenian Sea: an overview of 30 years of research. Mar. Geol. 204, 161–185.

Elderfield, H., 1988. The oceanic chemistry of the rare earth elements. Philos. Trans. R. Soc. Lond., A 325, 105–126.

Francalanci, L., Manetti, P., 1994. Geodynamic models of the southern Tyrrhenian region: constraints from the petrology and geochemistry of the Aeolian volcanic rocks. Boll. Geofis. Teor. Appl. 36, 283–292.

Früh-Green, G.L., Kelley, D.S., Bernasconi, S.M., Karson, J.A., Ludwig, K.A., Butterfield, D.A., Boschi, C., Proskurowski, G., 2003. 30,000 years of hydrothermal activity at the Lost City vent field. Science 301, 495–498.

Füchtbauer, H., Goldschmidt, H., 1965. Beziehungen zwischen Calziumgehalt und Bildungsbedingungen der Dolomite. Geol. Rundsch. 55, 29–40.

Graf, D.L., Goldsmith, J.R., 1956. Some hydrothermal syntheses of dolomite and protodolomite. J. Geol. 64, 173–186.

Greaves, M.J., Rudnicki, M., Elderfield, H., 1991. Rare earth elements in the Mediterranean Sea and mixing in the Mediterranean outflow. Earth Planet. Sci. Lett. 103, 169–181.

Grousset, F.E., Parra, M., Bory, A., Martinez, P., Bertrand, P., Shimmield, G., Ellam, R.M., 1998. Saharan wind regimes traced by Sr–Nd isotopic composition of the Subtropical Atlantic sediments: last glacial maximum vs today. Quat. Sci. Rev. 17, 4–5.

Guerzoni, S., Chester, R. (Eds.), 1996. The Impact of Desert Dust Across the Mediterranean. Kluwer, Dordrecht. 389 pp.

Guerzoni, S., Lenaz, R., Quarantotto, G., Rampazzo, G., Correggiari, A., Bonelli, P., 1989. Trace metal composition of airborne particles over the Mediterranean Sea. G. Geol. 51/2, 117–130.

Gurvich, E.G., 2006. Metalliferous sediments of world ocean. Fundamental Theory of Deep-Sea Hydrothermal Sedimentation. Springer, Heidelberg. 420 pp.

Hamelin, B., Lambret, B., Joron, J., Treuil, M., Allegre, C.J., 1979. Geochemistry of basalts from the Tyrrhenian Sea. Nature 278, 832–834.

Hamelin, B., Grousset, F., Biscaye, P.E., Zindler, A., 1989. Lead isotopes Trade Wind aerosols at Barbados: the influence of European emissions over North Atlantic. J. Geophys. Res. 94, 16243–16250.

Hekinian, R., Hoffert, M., Larqué, P., Cheminée, J.L., Stoffers, P., Bideau, D., 1993. Hydrothermal Fe and Si oxyhydroxide deposits from south Pacific intraplate volcanoes and East Pacific Rise axial and off-axial regions. Econ. Geol. 88, 2099–2121.

Hieke, W., Glaçon, G., Hasegawa, S., Müller, C., Peypouquet, J.P., 1990. Sedimentation in the Marsili Basin during Quaternary (ODP Site 650, Tyrrhenian Sea). In: Kastens, K.A., Mascle, J., et al. (Eds.), Proc. ODP, Sci. Results, vol. 107, pp. 255–289.

Hoogakker, B.A.A., Rothwell, R.G., Rohling, E.J., Paterne, M., Stow, D. A.V., Herrle, J.O., Clayton, T., 2004. Variations in terrigenous dilution in western Mediterranean Sea pelagic sediments in response to climate change during the last glacial cycle. Mar. Geol. 211, 21–43.

Juteau, M., Michard, A., Albarede, F., 1986. The Pb–Sr–Nd isotope geochemistry of some recent circum-Mediterranean granites. Contrib. Mineral. Petrol. 92, 331–340.

Kamenov, G.D., Mueller, P.A., Perfit, M.R., 2004. Optimization of mixed Pb–Tl solutions for high precision isotopic analyses by MC-ICP-MS. J. Anal. At. Spectrom. 19, 1262–1267.

Kamenov, G.D., Perfit, M.R., Jonasson, I.R., Mueller, P.A., 2005. High-precision Pb isotope measurements reveal magma recharge as a mechanism for ore deposit formation: examples from Lihir Island and Conical Seamount, Papua New Guinea. Chem. Geol. 219, 131–148.

Kastens, K.A., Mascle, J., Auroux, C., et al., 1987. Proc. ODP, Init. Repts., vol. 107. Ocean Drilling Program, College Station, TX.

Kelley, D.S., Karson, J.A., Blackman, D.K., Früh-Green, G.L., Butterfield, D.A., Lilley, M.D., Olson, E.J., Schrenk, M.O., Roe, K.K., Lebon, G.T., Rivizzigno, P., the AT3-60 Shipboard Party, 2001. An off-axis hydrothermal vent field near the Mid-Atlantic Ridge at 30° N. Nature 412, 145–149.

Kelley, D.S., Baross, J.A., Delaney, J.R., 2002. Volcanoes, fluids, and life at mid-ocean ridge spreading centers. Annu. Rev. Earth Planet. Sci. 30, 385–491.

Kelley, D.S., Karson, J.A., Früh-Green, G.L., Yoerger, D.R., Shank, T.M., Butterfield, D.A., Hayes, J.M., Schrenk, M.O., Olson, E.J., Proskurowski, G., Jakuba, M., Bradley, A., Larson, B., Ludwig, K., Glickson, D., Buckman, K., Bradley, A.S., Brazelton, W.J., Roe, K., Elend, M.J., Delacour, A., Bernasconi, S.M., Lilley, M.D., Baross, J.A., Summons, R.E., Sylva, S.P., 2005. A serpentinite-hosted ecosystem: the Lost City hydrothermal field. Science 307, 1428–1434.

Krom, M.D., Cliff, R.A., Eijsink, L.M., Herut, B., Chester, R., 1999. The characterization of Saharan dusts and Nile particulate matter in surface sediments from the Levantine basin using Sr isotopes. Mar. Geol. 155, 319–330.

Land, L.S., 1985. The origin of massive dolomite. J. Geol. Educ. 33, 112–125.

Löye-Pilot, M.D., Martin, J.M., Morelli, J., Gros, J.M., Strauss, B., 1986. Impact des poussières sahariennes sur l'acidité des pluies

dans l'atmosphère méditerraneene. Proc. Fourth European Symp., Stresa, Italy, 23–25 September 1986, pp. 489–499.
Lumsden, D.N., 1979. Discrepancy between thin section and X-ray estimates of dolomite in limestone. J. Sediment. Petrol. 49, 429–436.
Marchig, V., Gundlach, H., Möller, P., Schley, F., 1982. Some geochemical indicators for discrimination between diagenetic and hydrothermal metalliferous sediments. Mar. Geol. 50, 241–256.
Martin, J.H., 1990. Glacial-interglacial CO2 change: the iron hypothesis. Paleoceanography 5, 1–13.
Matthews, A., Katz, A., 1977. Oxygen isotope fractionation during the dolomitization of calcium carbonate. Geochim. Cosmchim. Acta 41, 1431–1438.
Mayers, W.J., Lu, F.H., Zacharian, J.K., 1997. Dolomitiozation by mixed evaporative brines and freshwater, upper Miocene carbonates, Nijar, Spain. J. Sediment. Res. 67, 898–912.
McKenzie, J.A., Isern, A., Karpoff, A.M., Swart, P.K., 1990. Basal dolomitic sediments, Tyrrhenian Sea, Ocean Drilling Program Leg 107. In: Kastens, K.A., Mascle, J., et al. (Eds.), Proc. ODP, Sci. Results, vol. 107, pp. 141–152.
McLennan, S.M., 1989. Rare earth elements in sedimentary rocks: influence of provenance and sedimentary processes. In: Lipin, B.R., McKay, G.A. (Eds.), Geochemistry and Mineralogy of Rare Earth Elements. Rev. Miner., vol. 21, pp. 169–200.
McMurtry, G.M., Sedwick, P.N., Fryer, P., VonderHaar, D.L., Yeh, H.W., 1993. Unusual geochemistry of hydrothermal vents on submarine arc volcanoes: Kasuga Seamounts, Northern Mariana Arc. Earth Planet. Sci. Lett. 114, 517–528.
Mottl, M.J., 1983. Metabasalts, axial hot springs, and the structure of hydrothermal systems at mid-ocean ridges. Geol. Soc. Amer. Bull. 94, 161–180.
Murray, R.W., Brink, M.R.B., Gerlach, D.C., Russ III, G.P., Jones, D.L., 1991. Rare earth, major and trace elements in chert from the Franciscan Complex and Monterey Group, California: assessing REE sources to fine grained marine sediments. Geochim. Cosmochim. Acta 55, 1875–1895.
Nebout, N.C., Grazzini, C.V., 1991. Late Pliocene Northern Hemisphere glaciations: the continental and marine responses in the central Mediterranean. Quat. Sci. Rev. 10, 319–334.
Petit, J.-R., Briat, M., Royer, A., 1981. Ice age aerosol content from East Antarctic ice core samples and past wind strength. Nature 293, 391–394.
Pye, K., 1987. Aeolian Dust and Dust Deposition. Academic Press. 334 pp.
Rea, D.K., 1994. The paleoclimatic record provided by eolian deposition in the deep sea: the geologic history of wind. Rev. Geophys. 32, 159–195.
Robertson, A.H.F., 1990. Pliocene basal dolomitic and Fe–Mn sediments from the Tyrrhenian Sea, Western Mediterranean, ODP Leg 107. In: Kastens, K.A., Mascle, J., et al. (Eds.), Proc. ODP, Sci. Results, vol. 107, pp. 129–139.
Rosenbaum, J., Sheppard, S.M., 1986. An isotopic study of siderites, dolomites and ankerites at high temperatures. Geochim. Cosmochim. Acta 50, 1147–1150.
Sarnthein, M., 1978. Sand deserts during glacial maximum and climatic optimum. Nature 272, 43–46.
Savelli, C., 1988. Late Oligocene to Recent episodes of magmatism in and around the Tyrrhenian Sea: implications for the processes of opening in a young inter-arc basin of intra-arc-orogenic (Mediterranean) type. Tectonophysics 146, 163–181.
Savelli, C., Gasparatto, G., 1994. Calc-alkaline magmatism and rifting of the deep-water volcano of Marsili (Aeolian back-arc, Tyrrhenian Sea). Mar. Geol. 119, 137–157.
Seewald, J.S., Seyfried Jr., W.E., 1990. The effect of temperature on metal mobility in subseafloor hydrothermal systems: Constraints from basalt alteration experiments. Earth Planet. Sci. Lett 101, 388–403.
Sun, S.-S., McDonough, W.F., 1989. Chemical and isotopic systematics of oceanic basalts: implications for mantle composition and processes. In: Saunders, A.D., Norry, M.J. (Eds.), Geol. Soc. London, Spec. Publ., vol. 42, pp. 313–345.
Taylor, S.R., McLennan, S.M., 1981. The composition and evolution of the continental crust: rare earth element evidence from sedimentary rocks. Philos. Trans. R. Soc. A 301, 381–399.
Tucker, M.E., Wright, V.P., 1990. Carbonate Sedimentology. Blackwell, Oxford. 482 pp.
Usui, A., Bau, M., Yamazaki, T., 1997. Manganese microchimneys buried in the Central Pacific pelagic sediments: evidence of intraplate water circulation? Mar. Geol. 141, 269–285.
Vergnaud-Grazzini, C., 1985. Mediterranean late Cenozoic stable isotope record: stratigraphic and paleoclimatic implications. In: Stanley, D.J., Wezel, F.C. (Eds.), Geological Evolution of the Mediterranean Basin. Springer, New York, pp. 413–451.
Von Damm, K.L., 1990. Seafloor hydrothermal activity: Black smoker chemistry and chimneys. Annu. Rev. Earth Planet. Sci. 18, 173–204.
Weaver, C.E., 1960. Possible uses of clay minerals in search for oil. Bull. Am. Assoc. Pet. Geol. 44, 1505–1518.